R and D TARADCOM LABORATORY

TECHNICAL REPORT

NO. 12258

VEHICLE VULNERABILITY TO LASER SYSTEMS

Contract: DAAE07-75-A-0508

January 1977

by Dr. William S. Chan
Michigan Technological University
Keweenaw Research Center, Houghton, MI

U.S. ARMY TANK-AUTOMOTIVE
RESEARCH AND DEVELOPMENT COMMAND
Warren, Michigan 48090

VEHICLE VULNERABILITY TO LASER SYSTEMS

ABSTRACT:

Vulnerability analyses were performed on the combat vehicles of M48A1 - tank, M113APC - personnel carrier, and M35A - truck, with the view of identifying the parameters relevant to the deployment of countermeasures.

The analysis of material damage caused by laser weapons showed that the currently-available high-power lasers posed no greater threat than conventional weapons, even though the on-board optical and imagery systems were vulnerable to being destroyed at short ranges and to being saturated at long ranges under direct irradiation.

The analyses of vulnerability related to rangers and designators were carried out by taking into account of the atmospheric extinction (μ), surface reflectivity (s), and angle of incidence (θ). The results were presented in the form of numerical computations of the reflected power under various conditions of μ, s, and θ, which, in turn, were identified as parameters amenable to being controlled for passive countermeasure deployment.

REPORT DOCUMENTATION PAGE

READ INSTRUCTIONS BEFORE COMPLETING FORM

1. REPORT NUMBER: TR-12258	2. GOVT ACCESSION NO.
3. RECIPIENT'S CATALOG NUMBER	
4. TITLE (and Subtitle): VEHICLE VULNERABILITY TO LASER SYSTEMS	5. TYPE OF REPORT & PERIOD COVERED: Final
6. PERFORMING ORG. REPORT NUMBER	
7. AUTHOR(s): Dr. William S. Chan	8. CONTRACT OR GRANT NUMBER(s): DAAE07-75-A-0508
9. PERFORMING ORGANIZATION NAME AND ADDRESS: Michigan Technological University, Houghton, MI 49931, Keweenaw Research Center	10. PROGRAM ELEMENT, PROJECT, TASK AREA & WORK UNIT NUMBERS
11. CONTROLLING OFFICE NAME AND ADDRESS	12. REPORT DATE: January 1977
	13. NUMBER OF PAGES: 90
14. MONITORING AGENCY NAME & ADDRESS (if different from Controlling Office): U.S. Army Tank Automotive Research and Development Command, Warren, MI 48090, Science & Technology Div. (DRDTA-RH)	15. SECURITY CLASS. (of this report): UNCLASSIFIED
	15a. DECLASSIFICATION/DOWNGRADING SCHEDULE

16. DISTRIBUTION STATEMENT (of this Report)

Approved for public release, distribution unlimited.

17. DISTRIBUTION STATEMENT (of the abstract entered in Block 20, if different from Report)

18. SUPPLEMENTARY NOTES

19. KEY WORDS (Continue on reverse side if necessary and identify by block number)

Laser weapons
Vehicle vulnerability
Countermeasures

20. ABSTRACT (Continue on reverse side if necessary and identify by block number)

Vulnerability analyses were performed on the combat vehicles of M48A1 - tank, M113APC - personnel carrier, and M35A - truck, with the view of identifying the parameters relevant to the deployment of countermeasures.

The analysis of material damage coused by laser weapons showed that the currently available high-power lasers posed no greater

threat than conventional weapons, even though the on-board optical and imagery systems were vulnerable to being destroyed at short ranges and to being saturated at long ranges under direct irradiation.

The analyses of vulnerability related to rangers and designators were carried out by taking into account of the atmospheric extinction (u), surface reflectivity (s), and angle of incidence (0). The results were presented in the form of numerical computations of the reflected power under various conditions of u, s, and 0, which, in turn, were identified as parameters amendable to being controlled for passive countermeasure deployment.

TECHNICAL REPORT

VEHICLE VULNERABILITY TO LASER SYSTEMS

Submitted to

U.S. Army Tank-Automotive Research and Development Command
Warren, Michigan 48090

Contract No. DAAE-07-75-A-0508
Delivery Order No. 0014

By

William S. Chan

Electrical Engineering Department

And

Keweenaw Research Center
Michigan Technological University
Houghton, Michigan 49931

Research Assistants

Jarm T. Wan
Thomas A. Lindsay

January 1977

SUMMARY

Initially, a gross-featured vulnerability analysis is carried out in terms of the amount of exposed parts of the vehicle's exterior that are vulnerable to damage by high-power lasers. These parts constitute about 21%, 10%, and 37% of the total surface area of the M48A1, M113APC, and M35A, respectively. An analysis on the capability of high-power lasers in inflicting material damage and destruction on the basis of melting and vaporization reveals that the currently available high-power lasers (over MW but less than GW) pose no greater threat than convention weapons at ranges greater than 10^3 meters.

On-board optical and imagery systems are only vulnerable if they are directly irradiated by high-power lasers at short ranges, but the probability of such a direct irradiation is low. At longer ranges or with less powerful lasers (e.g. rangers and designators), a direct irradiation might cause temporary saturation of IR detectors and photocathode multipliers without material damage.

All vehicles are vulnerable to laser rangers and designators, and the actual range in which they are vulnerable is dependent upon the emitted laser power, the scattering characteristic of the surface, the scattering property of the intervening atmosphere, and the divergence of the laser beam. Analyses are performed on reflected power from (1) diffused surfaces with area greater and smaller than the beam area, (2) reflecting surfaces with area greater and smaller than the beam area, (3) multi-faceted surfaces with area greater and smaller than the beam area. Using the results of these analyses and employ-

ing a GaAs 10 W laser numerical computations of reflected power from the different surfaces and from the three vehicles are carried out for various conditions of range, angle of incidence, surface scattering, atmospheric absorption, and angle of elevation.

The results of the analyses show that there are only three parameters (atmospheric extinction coefficient (μ), surface reflectivity (s), and angle of incidence or angle of surface orientation to the beam ($\emptyset$)) which are controllable for passive countermeasure purposes. The parameter s is the most controllable and practical, and it can be made low in the form of surface coatings to minimize reflection for specific wavelengths of laser beams. The parameter μ is more dynamic, and it can be made high in the form of scattering screen about the vehicle. However, its dynamic character renders it practical only if the timing of providing the screen is coincident with the incidence of the laser beam, otherwise the effectiveness of the screen will be minimal under the dynamic condition of the vehicle, unless a permanent screen is applied. The parameter $\emptyset$ is the least practical since its alteration at the target by changing the orientation of surface plates etc. is only effective if the actual angle of incidence of the laser beam is known or anticipated.

It is recommended that further work be carried out to investigate the manner with which the parameters s, μ, and $\emptyset$ might be manipulated for countermeasures against rangers as well as for designators. In particular, numerical computations of designating power, angle of incidence, angle of interception, range, and angle of elevation should be carried out for designating vulnerability in detail along with an analysis and selection of countermeasure coatings. For

countering rangers and designators, the coatings should have reflectivities lower than 0.1 in the 1 micron spectral region. Preferably, the coatings' reflectivities should blend with those of the background environment.

TABLE OF CONTENTS

LIST OF FIGURES

LIST OF TABLES

1. INTRODUCTION

1.1 Objectives and Scope:

Combat ground vehicles are vulnerable to all manners of designation and attack from enemy sources. Recent advances in laser technology pose an added dimension of vulnerability to laser systems capable of ranging, designating, and attacking these vehicles with great accuracy. The survivability of vehicles depends, in great measures, on their ability to counter and thus to negate or to minimize the laser capabilities. In order to counter, the vulnerability aspects must be assessed. The primary objective of the present work is the first-order assessment of vulnerability aspects of the combat ground vehicles, and the specific objectives are:

(1) vulnerability of vehicles subject to power laser attack,

(2) vulnerability of on-board IR and laser detecting systems,

(3) vulnerability of vehicles subject to laser ranging and designating,

(4) identification of potential countermeasure parameters.

1.2 Definition of Systems:

Three combat ground vehicles are used to aid the present work: M48A1 tank, M113APC personnel carrier, and M35A truck.

Power laser systems are those whose primary beams are sufficiently powerful to inflict damage to vehicles (power lasers may also be used as rangers and designators).

Laser rangers are those whose reflected beams are received at the original source location, and whose primary function is to measure the range between the laser source and the target vehicle. (Rangers may be used to guide attacking missiles.)

Laser designators are those whose reflected beams are detected at any other location rather than at the source location, and whose primary function is to provide a designating beam continuously for guiding a missile attack on the vehicle target or for illuminating the vehicle target.

It is noted, however, other variant functions of the laser systems are possible, depending on their complexity and advancement in development, but for the purposes of the first-order assessment of vulnerability in the present work, the above definitions are assumed.

2. VULNERABILITY OF VEHICLES SUBJECT TO POWER LASERS

2.1 Surface Area Vulnerability

A gross-featured vulnerability analysis is performed in terms of the amount of the exposed area of the vehicle's exterior that is vulnerable to damage by power lasers, assuming they are capable of inflicting material damage. A more theoretical analysis is presented in a later section of this report on the actual capability of power lasers in material destruction, phase transformation, and penetration of material surfaces within the constraints of available power density and range of the laser beam. However, in the present section, we seek only a gross-featured understanding of the laser-vulnerable parts of the vehicles in, more or less, subjective terms so that these parts are identified for subsequent

detailed analysis if the need arises.

To carry out this gross-featured analysis, the different vulnerable parts are first classified under three headings:

A. Parts vulnerable and critical to vehicle operation. Parts are vulnerable because they are prominently exposed to the laser beam and because they are relatively weak in structure, and they are critical to vehicle operation because they have a direct function in the vehicle manueverability and defense and offense.

B. Parts vulnerable but not critical. These parts are considered not critical in the vehicle's manueverability and usefulness for defense and offense.

C. Parts not vulnerable. These are either relatively unexposed parts or highly armored parts that are virtually impervious to the most powerful laser available.

The classification is made by detailed visual inspection and by assuming the vehicles to be in a serviceable condition. Table 1 presents the summary of the classification.

For the gross-featured vulnerability analysis, the total area of each vehicle is first evaluated, and then the exposed vulnerable area is compared with the total to obtain a percentage which is termed as the percentage of vulnerability of the vulnerable part. Each vehicle is also analyzed in terms of different angles of incidence (relative to the horizontal plane) of the laser beam. Figures 1(a) and 1(b) are diagrams of the M48A1 and M113APC, respectively, showing the various views of the vehicles. A similar diagram for the M35A truck is given in Fig. 2.

Figures 3, 4, and 5 are plots of the vulnerable surface area of the M48A1, M113APC, and the M35A, respectively, with respect to the angle of rotation of the laser beam about the vehicle. In these plots, the angle of incidence of the laser beam is used as a parameter. It can be seen that there is a large variation of vulnerability at the different angle of rotation. Also, it appears that the vehicles are most vulnerable to the incident laser beam whose direction is about 45^{o} to the horizontal plane (i.e. 45^{o} elevation). This is so because at this angle the vehicles offer the maximum surface area for beam impingement.

In summarizing the results of figures 3 to 5, table 2 presents the percentages of vulnerability for the three vehicles studied. It is noted in the analysis that only the type A parts are considered.

2.2 Personnel Vulnerability

All personnel associated with vehicles are vulnerable[1-5] if they are exposed to power laser attack. Their vulnerability is no more severe than that associated with conventional weapons. However, there are additional hazards that can be isolated. Personnel inside the M484A1 are vulnerable to scattered and direct laser beams which penetrate into the vehicle through viewing ports and periscopes. It is estimated on the basis of the size of these ports and apertures that the probability of beam penetration is about 1:1000. It follows that the probability of personnel irradiation is much lower than this figure. By considering the ratio of the irradiated area to the total wall area of the tank interior, it might be estimated that the

Table 1. Classification of Vulnerable Parts

Category		Vehicle		
		M48A1	M113APC	M35A
A.	Parts vulnerable and critical to vehicle operation	Track and pads Small guns Turret base Main gun Cupola windows Periscopes	Track and pads Machine gun Periscope Cupola base Latch on rear door	Gas tank Oil pan Radiator Batteries Tires Engine compartmer Cab Front and rear axle
B.	Parts vulnerable but not critical	Driving lamps Rubber on track rollers Fenders Mufflers Antenna Small turret vent Bussell Hatch lids	Driving lamps Rubber on rollers Antenna Windshield Mesh over engine Hatches and door	Driving lamps Exhaust Front fenders Water carriers Windshield
C.	Parts not vulnerable	Turret proper Metal over engine Cupola Main body Wheels Suspensions	Main body Rollers Main wheels Suspensions	Frame Bumpers Wheel rims Suspension

Table 2. Percentages of Vulnerability

	Surface View	% Vulnerability		
		M48A1	M113AP1	M35A
1.	Rear (0^{o} elevation)	26.7	9.3	31.3
2.	Left side (0^{o} elevation)	16.8	5.8	28.4
3.	Right side (0^{o} elevation)	16.8	5.8	31.8
4.	Front (0^{o} elevation)	26.7	14.5	25.6
5.	Top view (90^{o} elevation)	0.2	1.0	30.0
6.	Side view (45^{o} elevation)	12.8	---	----
7.	Total vulnerable area	20.8	10.1	36.5

probability of personnel irradiation is no more than $1:10^4$. Another hazard is that the penetrating beam might cause toxic evaporant with the confined vehicle interior. The probability of this happening (on the basis of area) is again about $1:10^4$, assuming paint vapor to be toxic. Similar figures of probability are estimated for the M113APC. Since the M35A has a great deal more penetratable ports and apertures, it is estimated that the probability of personnel irradiation is as high as 1:5. It is stressed that the above assessment is based on the probability of the laser beam penetrating windows, ports, etc.; no attempt has yet been made on destructability of the power laser.

2.3 Analysis of the Capability of Power Lasers

Much has been published in the open literature on the employment of power lasers for processing[6], and the effects of power lasers on material surfaces[7,8]; however, little study is made on the destructive nature of power lasers on combat vehicles. This is not too difficult to understand as the most advanced power lasers available with their attendant high power density are not yet capable of annihilating heavily armored vehicles, though they are capable of inflicting isolated damages on vulnerable parts. Even with the vulnerable parts, there is still the question of how much damage that can be inflicted by using currently available power lasers. To address this question, we set out to assess the capability of power lasers in terms of their effects on:

1. Melting of opaque surfaces,

2. Vaporization (phase transformation) of opaque surfaces

There are many power lasers currently available. Table 3 shows the parameters of three most commonly available lasers capable of producing high power density and are useful for weapons applications. The power ratings shown are typical but not the state-of-the-art figures.

By considering the energy transfer between the laser beam and the laser-irradiated surface area, a first-order analysis shows [9] that the temperature profile of the irradiated area can be described by the following equation:

$$T(r,z,t) = \left(\frac{d^2\, k^{1/2}\, F_o}{K\, \pi^{1/2}}\right) \int_o^t \frac{\exp(-z^2/4k\,t')\ \exp\left[\frac{-r^2}{(4k\,t'+d^2)}\right]}{t'^{1/2}\ (4k\,t'+d^2)}\, dt' \qquad -(1)$$

where d = radius of a Gaussian profile

k = thermal diffusivity

F_o = absorbed flux density at the surface

K = thermal conductivity of the surface

r = radial distance from the center of the irradiated spot

z = distance from the surface

t = time

TABLE 3. EXAMPLES OF HIGH-POWER LASERS

	Laser	Mode of Operation	Power (watt)	Pulse Width	Repetition Rate	(μ)
1.	Ruby	Q-switched	10^9 (p)	5-30 ns	low	0.694
2.	Nd-YaG	Q-switched	10^4 (p)	200 ns	5×10^3 p/sec	1.06
			10 (ave)			
3.	CO_2	continuous	$10 - 5 \times 10^3$			1.06
4.	CO_2	pulsed	10^5 (p)	10 - 100 μs	100 p/sec.	
			10^2 (ave)			

Equation (1) may be used to evaluate the penetration depth of melting of the irradiated surface. Numerical evaluation of material melting by using this equation shows only very small melting depths are possible, even with a most powerful laser currently available. For example, consider a high thermal conductive material such as copper of which the melted depth is only a fraction of a cm when a laser with flux density of about 10^6 w/cm^2 used, as illustrated in figure 6 which shows a plot of melted depth vs. pulse length of the laser beam.[8] Similar calculations may be made with other materials, and same order of magnitude of melted depth is obtained. In fact, equation (1) may be modified to evaluate melt depths for different materials. The maximum depth that may be melted without surface vaporization may be expressed by

$$\text{Xm (maximum melted depth)} = \frac{\text{G (material factor)}}{\text{F (laser flux density)}}$$

Table 4 is a tabulation of some common materials and their corresponding maximum melted depths calculated with a laser flux density of 10^6 w/cm^2.

Perhaps the most severe damage to a surface irradiated by power lasers is vaporization whose phenomenon is schematically depicted in figure 7 in which three stages of vaporization after irradiated by a laser pulse are shown. At the beginning of the pulse, vaporization takes place rather rapidly. When the pulse reaches its maximum power, a plasma is created on the surface which tends to absorb most of the laser energy, thus very little vaporization takes place during this part of the pulse. As the pulse decays, the material plasma drops in intensity and further vaporization

Table 4. Calculation[8] of melted depths of some common materials when a laser with a flux density of 10^6 w/cm^2 is used

Material	C (material factor) w/cm	X_m (maximum melted depth) cm
Cu	7650	0.0077
Fe	1100	0.0011
Ni	2070	0.0021
W	4650	0.0047

again takes place. It can be seen that the characteristic of the laser pulse is an important parameter in determining the vaporization of a surface.

To evaluate the damage made on a material surface by vaporization, calculation on the amount of material removed from the irradiated surface may be made. It can be shown[8] that when the material is exposed to a constant flux, the rate (r_v) of material removal by vaporization is given by:

$$r_v = (F/\rho)\,[L + C\,(T_v - T_o)], \qquad -(2)$$

where F = flux density

C = heat capacity per unit mass

ρ = density

T_o = initial temperature

T_v = vaporization temperature

L = specific heat of vaporization per unit mass

Another parameter important to the calculation of vaporization depth is the time (t_v) required to raise the irradiated surface to its vaporization temperature (T_v):

$$t_v = \left(\frac{\pi}{4}\right)\left(\frac{k\rho c}{F^2}\right)(T_v - T_o)^2 \qquad -(3)$$

This time (t_v) is generally short,[9] for many materials t_v may be comparable to the pulse duration of the laser, in which case vaporization is only possible with very high flux density and at the later part of the pulse duration. It appears, therefore, that significant amount of material damage by vaporization is only possible with continuous irradiation or with long pulse duration. Analysis has been carried out[9] on the vaporized depth for several materials by employing

(2) and (3) and considering the occurrence of vaporization between t_v and the end of the laser pulse. Figure 8 shows some results of the analysis, using a pulse duration of 700 microseconds. It can be seen that, even with very high flux densities, the vaporized depths are less than 1 cm for all the materials considered.

Other effects such as changes in surface reflectivity[10] and the occurrence of surface explosion[11] are possible when a surface is irradiated with power laser. These are inconsequential as far as vehicle vulnerability is concerned as surface explosions are minute compared to battle explosions; surface explosions usually originate from eruption of boiling and vaporization of the surface materials.

One conclusion may be drawn from the analysis of melting and vaporization is that power lasers which are currently available are not capable of inflicting substantial material damage on heavily armored surfaces. However, side effects and less heavily structured surface parts may still render the combat vehicle vulnerable. For example:

1. Continuous high-power laser irradiation is possible and can inflict substantial surface damages which may cause weakening of surface structures which, in turn, become highly vulnerable to destruction by conventional weapons under actual battle conditions.
2. Instrumentation and on-board signal or laser detecting devices are all highly vulnerable to power laser destruction if they are

directly irradiated. This aspect of vulnerability is considered in the next section of this report.

(3) Power lasers can easily induce toxic fumes by vaporization of some surface materials which normally are non-toxic.

3. VULNERABILITY OF ON-BOARD OPTICAL AND IMAGERY SYSTEMS

As pointed out in the last two sections, the most vulnerable parts in combat vehicles are those optical or imagering systems which may be directly irradiated by lasers through ports, periscopes, and other viewing apertures. Though the probability of these being irradiated is low from the exposed surface area point of view, they are nevertheless vulnerable to the extent of rendering ineffectual use of vehicles in combat, as they function as "eyes" and "ears" and "aim" in vehicle deployment. Further, their vulnerability is heightened by the high probability of being completely destroyed if they are directly irradiated.

The currently deployed on-board optical and imagery systems include IR image converter tubes, image intensifiers, FLIR systems, optical filters, range finders, and radiation detectors. For the purpose of assessing their destructibility when irradiated, each system (except filters) may be represented by several essential structural parts, as shown in figure 9. This figure shows the approximate order of vulnerability to irradiation with the component (system housing) to the extreme left being the most vulnerable, and the component (amp and display electronics) to the extreme right being the least vulnerable. It is to be noted that the components of the filters, the anti-reflection coatings, and the detector element are invariably one integral

system. As descriptions and performances of the optical and imagery systems are well documented in the literature [12], we will not go into them in detail, except those factors which are relevant to our assessment of vulnerability.

Consider the system housing first. Its essential functions are:

1. to provide environmental protection to the detector element, filters, and the anti-reflection coating (sometimes to the transducer and preamp. electronics as well).
2. to provide (in most systems) a vacuum environment for the proper function of the detector element.
3. to provide containment of a liquid or electrical (thermoelectric cooler) coolant for the proper function of the detector element.
4. to provide a transparent front end for the reception of radiation signals.

Since the front end is usually designed with high transparency to radiation to be detected by the detector element, therefore the amount of laser radiation being absorbed by the front end in this particular spectral region appears not sufficient to cause damage, except for extreme high flux densities or for highly absorbing front ends. This appears to be not the case as work done in this field [13] has shown that much damage can occur when a powerful laser beam passes through a transparent material. In most of the optical and imagery systems mentioned above, the front end is usually transparent

to most of the laser systems available. Therefore, the analysis of front-end damage may be treated as laser damage in transparent materials. A great deal has been published on mechanisms of damage in transparent materials [14], but much is still contradictory. The major mechanisms of damage may be described as follows:

1. A combination of the stimulated Brillouin[15] scattering and the coherent generation[16] of intense hypersonic waves produces an electrostrictive strain which, in turn, causes damage in the form of cracks and shattered surfaces.
2. Multiphoton absorption[17] process excites electrons into a high-lying conduction band which facilitates the impact ionization of these electrons in the field of the laser radiation causing a plasmic breakdown. The damage is usually in form of a chain of ringlike microscopic fractures.
3. Absorption of laser radiation by defects or material inhomogeneities[18] causes melting or vaporization which leads to thermal destruction of the transparent material.

All these mechanisms can operate in unison or independently to cause damage, and they are highly power dependent. The production of damage under specified conditions occurs when the laser power exceeds a certain threshold value characteristic of material.[19] The threshold value of the material used for construction of the front end of the system housing is a first-order parameter for assessing the vulnerability of the front end. For example,

Table 4 shows a listing of threshold values of some commonly available glasses. It is noticed that the purer the glass the higher the threshold, as expected from the defect-absorption mechanism.

Damage, but not complete destruction, of the front end leads to lowering of detector performance and shortening of the life cycle of the whole system. In the extreme, complete destruction of the front end leads to the following possibilities:

1. Loss of environmental and vacuum protection at the very least
2. Loss of cooling, thus lowering the performance of the detector element or rendering it useless
3. Production of misleading or erroneous information

As far as the power laser is concerned, the filters, anti-reflection coatings, and the detector element are most vulnerable parts of the whole system because most of the laser power is being absorbed by these parts. Since most filters are multiple-layer, narrow-band-pass type, therefore, high absorption of the laser beam may take place within these filters, and the thermal types (melting and vaporization) of damage mechanism appear to dominant. However, other mechanisms such as defect absorption etc. can also be effective. This means that the filters can be damaged more easily than the front end. It is possible that lower power lasers may be able to inflict sufficient damage to render the filters useless. Filter damage leads to the following possibilities:

Table 5. Thresholds in glasses for Q-switched laser pulses

Type	Threshold (GW/cm^2)
Borosilicate crown	710
Barium crown	710
White crown	500
VYCOR	490
SiO_2 glass	470
Annealed aluminosilicate	15.4
Tempered borosilicate gage	6.0
Quartz glass	2.4
Lanthanum borate glass	2.0

1. Complete loss of band-pass transparency; therefore, the detector element becomes virtually useless.
2. Partial or complete alteration of the filtering produces considerable or disappearance of detector performance.
3. The destruction of filters will most likely result in destruction of anti-reflection coatings and detector.

Anti-reflection coatings are usually integral parts of the radiation detectors. They would most likely to suffer thermal types of damage, and their destruction would lead, at least, to considerable lowering in detector performance.

Most of the detectors deployed in optical and imagery systems (such as FLIR, IR detectors, and range finders) are semiconductor quantum or photocathodes (photomultipliers) devices. Photocathodes are extremely sensitive to damage by a high incident photon flux density. Power lasers can completely destroy the low work-function cathode coating (such as cesium). Since cathodes are high absorbers of radiation, they would be highly vulnerable to thermal types of damage (melting and vaporization), even when low-power beams (5 joule/cm^2) are used on them. This means that photomultipliers are highly vulnerable to laser damage.

Laser damage in semiconductor devices can occur in two regimes, one is that the semiconductors are considered as opaque absorbers whose absorption edge is greater than the wavelength of the incident laser radiation, and the other is that the semiconductors are considered transparent to the incident beam. Many investigations[20-22] on damage have shown that the

former is the dominant damage mode, even when the semiconductors are transparent, in which case impurity absorption would induce thermal types of damage .

The absorption mechanism in highly absorbing semiconductors is the creation of free electron-hole pairs which on recombination give up energy to heat up the whole crystal lattice, and, in so doing dislocation, melting, and eventual destruction of the semiconductor crystal lattice can occur. For example[21], a ruby laser pulse inflicts considerable damage in Ge, Si, GaAs, InSb, and CdSe. When energy densities are low (5-10 joule/cm^2), surface damage is visible under a microscope, indicating some form of phase transformation. As energy density increases (greater than 10 joule/cm^2), crack lines and thermal etch pits are manifested. At higher density (greater than 20 joule/cm^2), severe craters are formed. More powerful pulses (200 kW/cm^2) can cause electron-hole plasma[23] with plasma density greater than $10^{18}/cm^3$.

Consider two specific semiconductors, Si and InSb, which are commonly deployed in the form of avalanche photodiode detector and of photovoltaic IR detector, respectively. Si avalanche photodiodes are very important radiation detectors used in conjunction with laser rangers in the 1.08 and 0.9 micron spectral regions (in the range of Nd laser and GaAs laser, respectively). InSb photovoltaic detectors are the most sensitive detectors in the 3 to 5 micron spectral range, and are well proven devices for FLIR and night vision military applications. The nature of some of the damages on InSb

devices that can be inflicted by power lasers has been indicated in the above paragraph. However, when less powerful lasers (such as those employed in laser rangers and designators) are used on InSb detectors, saturation and other secondary effects (thermal damage aside) can take place which will cause a loss of sensitivity. Three such effects are highly possible:

1. Production of non-linear photoresponse, causing substantial drop in detectivity. The work of Hammond and Stanley [24] touched upon this problem in their work on irradiating InSb with a high intensity 5.3 micron laser.
2. High incident photon flux causes high injection of charge carriers across the photovoltaic junction. By itself, this process may not directly cause a drop in detectivity, but since most optimization of InSb detector performance is invariably based on the low injection[25] approximation, and a significant change in detector output characteristic does take place under high injection, mismatch between detector and amplifying electronics will then occur resulting in performance lowering.
3. High incident photon flux at the photodiode junction creates a high density of electron-hole pairs which tend to neutralize the space charge of the junction. When the degree of neutralization begins to decrease the potential barrier of the junction significantly, saturation of the photocurrent sets in, resulting in the disappearance of detectivity and response time of the detector. The photon flux density required for saturation is

analyzed using a simplified junction model [26] in the following way.

A high photon flux produces a photo voltage (V_f) at the junction which tends to forward bias the diode. As V_f increases with increase in photon flux saturation sets in when V_f approaches the contact potential (V_o) of the junction. It can be shown [26] that the photon flux per second per unit area (ϕ, no. quanta/sec/cm^2) is related to V_f by:

$$\phi = \frac{A_o \left[\exp\left(\frac{q\,V_f}{kT}\right) - 1\right]}{(V_o - V_f)^{1/2}}$$

where A_o = constant related to the material parameters of the semiconductors of the diode

k = Boltzmann's constant

T = temperature

It can be seen that as ϕ approaches infinity, V_f approaches V_o. Using the materials parameters in Table A.1, given in appendix 1, it is estimated that the photon flux density per second required to increase V_f to 90% of V_o is about 1.3×10^{18} photon/sec/cm^2, which corresponds to an irradiance of 4.9×10^{-2} watt/cm^2. If a 5.3 μ laser with a divergence of 1×10^{-3} radian were used to saturate the InSb detector at a range of 500 meters, the power of this laser had to be about 100 watts. Obviously, at shorter ranges much lower power is sufficient to saturate. This analysis (see Appendix A2) shows that medium-level power lasers are capable of saturating InSb IR detectors at kilometer ranges, even

though they are not capable on inflicting thermal damages.

Silicon avalanche (or other type) photon detectors are saturable by power lasers, but it can be followed from the argument given in Appendix A. 2 that much higher laser power is required to saturate Si type of detectors on the basis of the materials parameters and the higher energy band gap and contact potential. It follows that Si devices are not as vulnerable to saturation as InSb devices. Further, if the power is high enough for saturating Si devices, it is likely to be high enough for thermal damages previously described. The work of Yoshihara Matsuoka[27] on laser damage of silicon cells indicates that the threshold power density in the order of 10 MW/cm^2 is required to lower the photocurrent, and at this level of power density surface damage is already visible to the naked eye.

Summary of section 2.4 is as follows:

(1) On-board optical and imagery systems are the most vulnerable parts of the vehicle system if they are directly irradiated by power lasers.

(2) The damage of these systems are high power dependent, therefore, range dependent.

(3) The types of damages alludes to are not likely to occur if the ranges are great (greater than 10^3 meters). At smaller ranges, all optical-related systems are vulnerable. For example, a 10^{10} watt

laser at a range of 1 km and having a divergence of 2×10^{-3} radian will produce an irradiance of about 500 watt/cm^2. Such power density is sufficient to cause thermal damages to all detector materials.

(4) InSb and other similar types of IR detectors are more vulnerable to saturation and lowering of sensitivity than Si type of devices at medium power levels and at longer ranges.

4. VULNERABILITY OF VEHICLES SUBJECT TO RANGERS AND DESIGNATORS

4.1 General Description of Reflected Power

The capability of laser rangers and designators depends primarily on the reflected power (P_r) of the laser beam reflected from a given surface. In this section, attempt is made to analyze vehicle vulnerability in terms of parameters which directly influence the reflected power received by the ranger or designator detecting system. Typically, the ranger or designator is disposed to the vehicle target as depicted in Fig. 10. It can be seen that for rangers the receiver and transmitter are located at one location and are integral parts of the whole ranger system. For designators, the transmitter is the designator system, and the receiver may be located elsewhere and part of a separate detecting system.

The reflected power is highly dependent on the nature of the target surface which, in general, may be described by a scattering function $F(\phi_t, \phi_r)$, where ϕ_t and ϕ_r are the angles that the transmitter and receiver beams make with the target surface. Most naturally occurring targets have surface irregularities large compared with the laser wavelength and will scatter the radiation isotropically so that $F(\phi_t, \phi_r)$ is approximately constant for all

ϕ_t and ϕ_r. Thus, $F(\phi_t, \phi_r)$ is called the scattering coefficient of the surface and will vary from zero for a perfect absorber to unity for a loss-less surface. For artificially designed surfaces, $F(\phi_t, \phi_r)$ may have a specular as well as an isotropic component and an enhanced signal may occur at certain combinations of ϕ_t and ϕ_r. For a given vehicle, it is very difficult to analyze $F(\phi_t, \phi_r)$ realistically while making this function mathematically tractable. It is necessary, for accurate analysis, to make a direct measurement of $F(\phi_t, \phi_r)$ for the vehicle target. However, for the present work, we assume certain very simple models of surfaces in an attempt to obtain some assessment of vulnerability.

In general, the reflected power (P_r) for rangers and designators may be expressed in the following generic terms, neglecting the effects of polarization:

$$P_r = P_T [F_t \times F_r] \times [F(\phi_t, \phi_r)] \times [A_t \times A_r], \qquad -(1)$$

where

P_T = laser transmitted power

F_t = optical function of the transmitter

F_r = optical function of the receiver

$F_{(\phi_t, \phi_r)}$ = scattering function of the surface

A_t = atmospheric function of the transmitter

A_r = atmospheric function of the receiver

For both the designator and the ranger, the most important quantities are the scattering and the atmospheric functions, while the optical functions have no role to play in the minimization of P_r for the purposes of devising counter-

measures. The atmospheric functions describe the effects of the intervening space between the transmitter and target surface and between the receiver and the target surface, and are usually expressed as

$$A_t = \exp(-\mu_t R_t)$$

and $$A_r = \exp(-\mu_r R_r),$$

where μ_t = extinction (or absorption) coefficient of the atmosphere between receiver and target

μ_r = extinction coefficient of the atmosphere between transmitter and target

R_t = range between transmitter and target

R_r = range between receiver and target

It can be shown (see Appendix A3) that equation (1) may be specified fully by considering a Cosine-Lambertian type of scattering surface[28]:

$$P_r = P_T \left[\frac{4}{\pi\theta^2}\right][A_o T_o]\left[\frac{s A_s \cos\phi_t \cos\phi_r}{\pi R_t^2 R_r^2}\right][e^{-\mu_t R_t}][e^{-\mu_r R_r}] \qquad -(2)$$

where

θ = divergence of the laser beam

A_o = area of the receiver optics

T_o = transmittance of the receiver optics

A_s = area of the irradiated surface (may be smaller or greater than the beam area)

s = reflectivity of the surface

It is noted that if the surface is pure Lambertian (rather than Cosine-Lambertian), the term $\cos\phi_r$ in equation (2) drops out because the reflected power radiates into a hemisphere rather than into a cosine envelope.

4.2 Reflected Power Analysis of Cooperative Surfaces

Consider a ranger operating on a cooperative (non-diffused) surface; the reflected power received by the optics with area smaller than the reflected beam area is approximately given by:

$$P_r = P_T T_o s [1.75 (\cos \varphi + \varphi \sin \varphi - 1)] [\cos \gamma] e^{-2\mu_t R_t} \qquad -(3)$$

where

$$\varphi = \frac{r_o \pi}{2\theta R_t}$$

r_o = radius of the optics

$$\gamma = [\frac{\pi}{2} (\frac{\phi_t}{\theta/2})]$$

Equation (3) is derived (Appendix A3) by assuming a cosine approximation of the Gaussian distribution of the laser beam and a divergence defined by the 90% power points of this distribution.

Numerical computations of the reflected power are made by using a GaAs ranger having the following properties:

P_T = peak power of the GaAs laser

= 10 watt

θ = 5×10^{-3} radian

r_o = 3 cm

T_o = 80%

λ = 0.902 micron

The results of the computations are presented in figures 11 to 13 for different conditions of range, reflectivity, and atmospheric extinction

coefficient. It can be seen that the parameter μ (see fig. 13) can cause decrease in the reflected power and the range more substantially than other parameters can. Assuming the minimum reflected power required for detection to be about 10^{-8} watt[29] under day-time background condition, the maximum range that the target surface is vulnerable is about 6×10^4 meters.

Figure 12 shows plots of reflected power vs. range for different values of s. Figure 11 shows plots of reflected power vs. range for different divergence angles of the laser beam. From equation (3), it is noted that the receiver optics can receive only a fraction of the total reflected power, and only when the angle of incidence (ϕ_t) is smaller than the half divergence angle ($\theta/2$), otherwise no reflected power is received at all. This situation is more emphatically presented in Figure 14 in which the parameter ϕ_t is varied. An analysis is given in Appendix A3 of reflection from a retroreflective surface with the diameter of the received optics large enough to intercept totally the retroreflected beam. This situation is seldom encountered in ranging or designating of vehicle targets. However, the deployment of cooperative surfaces for countermeasures can be very effective against rangers (because of the terms φ and $\cos\left(\frac{\phi_t \pi}{\theta}\right)$) only if the angle of incidence (ϕ_t) is known, in which case the angle of orientation of the surface with respect to the beam direction may be altered to divert the reflected beam away from the ranger position. In reality, such use of ϕ_t for countermeasures is rather impractical, though not impossible, as it requires perfect anticipation of the direction of the incident beam.

4.3 Reflected Power Analysis of Non-Cooperative (diffused) Surfaces

The ranger reflected power from non-cooperative (diffused) surfaces may be specified as follows:

$$P_r = P_T [A_o T_o] [\frac{s \cos \phi_t}{\pi R_t^2}] e^{-2\mu_t R_t} \qquad -(4)$$

derived by assuming the Lambertian approximation and the surface area greater than the beam area. If the surface area is smaller than the beam area, the reflected power becomes:

$$P_r = P_T [\frac{4}{\pi \theta^2}] [A_o T_o] [\frac{s A_s \cos^2 \phi_t}{\pi R_t^4}] [e^{-2\mu_t R_t}] \qquad -(5)$$

Figures 15 to 17 are results of numerical evaluation of equations (4) and (5). It can be seen that considerably shorter ranges are obtained for the non-cooperative surfaces. Again, the parameter μ (fig. 15) has the substantial effect in the lowering of the reflected power and the range, but, now, the variation of the parameter s (fig. 16) can cause the reflected power to be detectable or not detectable. However, as it can be seen from figure 17, the angle of incidence becomes less sensitive in minimizing the reflected power. As far as countermeasures are concerned, the three parameters μ, s, and ϕ_t are within controllable limits in causing a lowering of the reflected power.

If a scattering screen around the surface is deployed, the reflected power may now be expressed:

$$P_r = P_T [\frac{4}{\pi \theta^2}] [A_o T_o] [\frac{s A_s \cos^2 \phi_t}{\pi R_t^4}] [e^{-2\mu_t R_t}] [e^{-2\mu_x R_x}] \qquad -(6)$$

where μ_x = atmospheric extinction coefficient of the scattering screen

R_x = thickness of the screen

Figure 18 shows plots of reflected power vs. range for different values of μ_x, assuming a screen thickness of 2 meters. In order to make a substantial lowering of reflected power or range, a high extinction coefficient is needed, as R_x is usually small compared with R_t and R_r.

Figure 19 are plots of reflected power vs. range for different values of transmitted power of laser rangers with μ set at 5×10^{-5} m^{-1}, s at 0.1, and angle of incidence at 0^o. These plots show the capability of different laser types with different transmitted power levels.

4.4 Reflected Power Analysis of n Multi-Surface Targets

If there are n surfaces being irradiated by the ranger laser beam and the ith surface is represented by a set of conditions (A_{si}, s_i, $\emptyset_i$, m_i), then the total reflected power received by the receiver optics is the sum of the reflected powers from the different surfaces. The reflection from a multi-surface target is a more realistic representation of the reflection from a vehicle target, as it constitutes many different surfaces. As described in Appendix A3, the factor m is used to compensate for effects of cluttering etc. and is usually about unity.

If the beam area is less than the projected area of the entire target of n visible surfaces, the reflected power received by the optics may be expressed:

$$P_T = \left(\frac{4\,P_T A_o T_o\, e^{-2\mu_t R_t}}{\pi^2 R_t^2\, \theta^2\, R_r^2}\right)\left[\sum_{i=1}^{n-1}(m_{fi} s_i A_i \cos^2\phi_i) + m_{fn} s_n \cos\phi_n \left(A_b - \sum_{y=1}^{n-1} A_y \cos\phi_y\right)\right] \quad -(7)$$

and, if the beam area exceeds the projected area of the target, then equation (7) reduces to

$$P_r = \left(\frac{4\,P_T A_o T_o\, e^{-2\mu_t R_t}}{\pi^2 R_t^2\, \theta^2\, R_r^2}\right)\left[\sum_{i=1}^{n} m_{fi} s_i A_i \cos^2\phi_i\right] \quad -(8)$$

4.5 Numerical Computations of Reflection Characteristics of the M48A1, M113APC, and M35A

Using equations (7) and (8) and the GaAs ranger laser, the reflection characteristics of the vehicles M48A1, M113APC, and M35A are computed. The results of computation are presented in figures 20-40, which may be briefly described as follows:

For the M113APC (Figures 19-25):

Fig. 20 - reflected power vs. range, when the side view of vehicle is irradiated, assuming s = 0.1, and for different values of atmospheric extinction coefficient

Fig. 21 - reflected power vs. range, when the side view of vehicle is irradiated, assuming $\mu = 5 \times 10^{-5}\ m^{-1}$, and for different values of reflectivity

Fig. 22 - reflected power vs. angle of rotation about vehicle (0^o is the front view), assuming $\mu = 5 \times 10^{-5}\ m^{-1}$ and s = 0.1, and for different angles of elevation (0^o elevation implies that the direction of the beam lies in the horizontal plane). It is noted that the side and top views are most vulnerable.

Fig. 23 - reflected power vs. angle of rotation about vehicle, assuming s = 0.1, angle of elevation of 0^{o}, and range at 500 meters, and for different atmospheric extinction coefficients

Fig. 24 - reflected power vs. angle of rotation, for different values of s (assuming $\mu = 5 \times 10^{-5}\ m^{-1}$, R = 500 meter, elevation = 0^{o})

Fig. 25 - reflected power vs. angle of rotation, for different values of R (assuming s = 0.1, $\mu = 5 \times 10^{-5}\ m^{-1}$, and elevation = 0^{o})

Fig. 26 - reflected power vs. range, for different views of vehicle (assuming s = 0.1 and $\mu = 5 \times 10^{-5}\ m^{-1}$)

For the M35A truck

Figs. 27-33 are similar plots as those for the M113APC, and explanations are contained in these plots.

For the M48A1 tank

Figs. 34-40 are also self-explanatory.

4.6 Threshold Detection

The detection of vehicle targets depends not only on the reflected power but also on the type of detecting and lasing systems used. Table 6 shows some common lasers used for rangers and designators. The two most important requirements of detectors used with these laser systems are sensitivity and speed of response. The kinds of detectors commonly used are photomultipliers, silicon PIN photodiodes, and, more recently, Si avalanche diodes.

The threshold of detection for each detector depends primarily on the predominant noise mechanism associated with the detector. Photomultipliers and avalanche diodes are background limited under high background radiation condition, for which the threshold number of photons (Δn_t) required for detection is given by[28]:

$$\Delta n_t = \left(\frac{s}{n}\right) \left(F_m \frac{d n_b}{dt} \frac{\Delta t}{E}\right)^{1/2} \qquad - (9)$$

where s/n = signal-to-noise ratio

F_m = noise factor associated with the multiplication process

$\frac{dn_b}{dt}$ = background photon flux scattered by the target and atmosphere

Δt = receiver response time (associated with the pulse width of the laser)

E = quantum efficiency of the detector

An analysis of $\frac{dn_b}{dt}$ has been made by Stitch[28], and an estimated plot of $\frac{dn_b}{dt}$ against field of view of the receiver is shown in figure (41).

Noise events can be treated on a statistical basis by assuming that these events, as well as the signal events, are independent and follow the Poisson distribution.[31, 32] Applying the Poisson statistics to typical rangers, it can be shown[28, 29] that in order to ensure a 0.99 probability of detection and a probability of false alarm of about 10^{-6} or less, a signal-to-noise ratio between 7 and 8 is required for target acquisition. In this report, when equations such as (9) are used to obtain estimates of threshold of detection, a signal-to-noise ratio of 7 is assumed.

When photomultipliers and avalanche diodes are used in low background conditions (night time), the dark current (I_D) noise is likely to predominate.[28] In this case, the threshold number of photons is given by[28]:

$$\Delta n_t = \left(\frac{s}{n}\right)\left(\frac{\Delta t\, F_m\, I_D}{q}\right)^{1/2}\left(\frac{1}{E}\right) \qquad -(10)$$

Detectors in the form of PIN photodiodes are usually Johnson noise limited[28], in which case their threshold of detection is related as:

$$\Delta n_t = \left(\frac{s}{n}\right)\left(\frac{I_f \Delta t}{qE}\right) \qquad -(11)$$

where I_f = rms effective noise current.

Once Δn_t is known, the actual threshold power (P_t) may be calculated according to the following expression:

$$P_t = \left(\frac{\Delta n_t}{\Delta t}\right)(hf) \qquad -(12)$$

where h = Planck's constant

f = frequency of the laser radiation

Sometimes the threshold power (P_t) may be estimated by using the detectivity (D^*) of the detector specified by the manufacturer:

$$P_t = \frac{(AB)^{1/2}}{D^*} \left(\frac{s}{n}\right) \qquad -(13)$$

where A = detector area

B = bandwidth.

However, equation(13)is insufficient to the extent that the field of view of the receiver, the predominant noise type, and the background condition are not fully specified by D^*.

Estimates of threshold Δn_t and P_t for typical photomultipliers, PIN photodiodes, and Si avalanche diodes are presented in Table 7 for conditions of:

λ = 0.902 μ (wavelength of laser)

$\Delta\lambda$ = 100 $\mathring{A}$ (spectral filter)

ω = 3 mr (field of view)

D = 6 cm (diameter of the receiver optics)

$\frac{dn_b}{dt}$(day time) = 10^{11} photons/sec

It can be seen that the lower limit of threshold of detection is about 10^{-8} watt. However, advances in Si avalanche diodes[33] may lower this figure further into the 10^{-9} watt range.

Table 6. Some Common Lasers used in Rangers and Designators

Laser Material	Class	Wavelength (μ)	Suitable Detector Type
Ruby ($Cr:Al_2O_3$)	solid-state	0.694	photomultiplier
Nd:yag	solid-state	1.06	Si photodiode or Si avalanche diode
GaAs	injection	0.906	same as above
GaAs P	injection	0.906	same as above
CO_2	gas	10.6	HgCdTe photovoltaic
N_2	gas	0.337	photomultiplier

Table 7. Estimated Threshold Power for Typical Detector Types in the 0.9μ Region(28)

Detector type	Quantum efficiency	F_m	Δt nsec	Threshold power (watt)	References
Photomultipliers	3×10^{-3}	4.3	15	1.5×10^{-7} (day time) 4.4×10^{-8} (night time)	(29)
Si avalanche diodes	0.5	4.6	20	2.2×10^{-8} (day time) 1.1×10^{-8} (night time, $I_D \sim 2 \times 10^{-9}$ A)	(28)
PIN photodiodes	0.5	---	20	2.7×10^{-7} (Johnson noise)	(28)

4.7 Scattering Parameters and Conclusions

The parameters μ, s, and $\emptyset$ are the main and controllable parameters for passive (limited active) countermeasures. Much has been studied[35] about natural and artificial atmospheric scattering, and deployment of μ for countermeasure is highly feasible, as seen in figures 13, 15, 20, 27, and 34 that substantial lowering of reflected power and range is possible, but the artificially-created atmospheric screens (figure 18) are necessarily dynamic in character in that the screens created around a vehicle will disappear after a period of time. As such, their deployment on vehicles will require a careful study of the anticipation of deployment and the degree of deployment. Since screen thicknesses are limited, high scattering and high absorption characteristics of the screening materials are needed. Obviously, the most effective screen is one that is designed specifically for the central wavelength of the ranging or designating laser. The parameter s is the most important countermeasure parameter as it is easily controllable and implemented. It is truly passive as it can be permanently applied in the forms of coating on the vehicle. The parameter $\emptyset$ is only partially controllable as it is dependent on the transmitter's angle of incidence; consequently, a structuring of the orientation of the vehicle surfaces in anticipation of the transmitter's direction is not very practical. However, orientational structuring may be effectively carried out if the most likely direction of incidence is known so that the initial few seconds of vehicle ranging or detection is minimized. The analyses above have shown that the isotropically-diffused surfaces are the best in minimizing the reflected power and in lowering the ranges.

Most of the detectors (photocathodes and Si photodiodes) employed with rangers are capable of a power threshold in the range of 10^{-8} to 3×10^{-7} watt in the 1μ region. Further improvement in the detector technology will likely extend the threshold to lower than 10^{-8} watt.

The main conclusions drawn from the numerical analyses are summarized as follows:

1. All vehicles are vulnerable to laser ranging and designating, even with low power lasers.
2. Vehicles are vulnerable up to at least 6×10^4 meters with currently available laser and detector technology. Higher ranges are possible with larger optics and powerful lasers.
3. Variation of reflected power is seen around vehicles, but the reflected power at all angles of incidence and elevation are detectable at short ranges (about 10^3 meters). At longer ranges, the variation can decrease the probability of detection.
4. Isotropically-diffused surface condition is best for minimizing the reflected power.
5. When long ranges (greater than 10^3m) are involved in designating and ranging, such that the laser beams "spill" substantially out of the vehicle target into the surrounding environment, it is advantageous to have the reflectivity of the target similar to the reflectivity of the surroundings. This condition can serve as a countermeasure by increasing the error of target acquisition by environmental scattering. Table 8 shows some typical reflectivities of naturally-occurred surfaces.

Table 8. Reflectivities of Some Naturally-Occurring Surfaces

Surface	Reflectivity [28]
Forest	
Coniferous (Summer)	0.13
(Winter)	0.03
Deciduous (Autumn)	0.30
(Summer)	0.16
Loam (Dry)	0.20
(Wet)	0.09
Sand (Dry)	0.43
(Wet)	0.32
Grass (Live)	0.14
(Dead)	0.26
Water (Specular)	0.02
Limestone (Clay)	0.71
Brown earth (Dry)	0.18
(Wet)	0.15
Red earth (Dry)	0.29
(Wet)	0.18
Barren terrain (Fresh tuff)	0.49
(Sandy)	0.13
Gravel	0.26
Snow	0.70

5. CONCLUSIONS

The main conclusion of this report may be summarized as follows.

(1) Vehicles are not highly vulnerable to high-power lasers, currently available, at ranges greater than 10^3 meters.

(2) At shorter ranges, power lasers will damage and destroy highly vulnerable parts of vehicles.

(3) These highly vulnerable parts constitute 20.8%, 10.1%, and 36.5% of the total surface area of the M48A1, M113APC, and M35A truck, respectively.

(4) On-board optical and imagery systems are the most vulnerable parts to complete destruction at short ranges, but the probability of laser penetration into the vehicle's interior is low, but not zero.

(5) Medium power lasers at short ranges can easily saturate InSb IR and similar detectors. But Si detectors are not so vulnerable.

(6) All vehicles are highly vulnerable to laser rangers and designators at ranges shorter than 10^3 meters.

(7) High-power rangers and designators will have longer ranges.

(8) The parameters μ, s, and $\emptyset$ are controllable and, therefore, feasible to be deployed for countermeasure purposes.

(9) The parameter μ is dynamic in character.

(10) The parameter $\emptyset$ has only limited applicability.

(11) The parameter s is most controllable and practical for countermeasure, especially for long ranges.

(12) Isotropically-diffused surfaces are recommended for countermeasures.

(13) Vehicles are vulnerable at all angles of incidence and elevation.

(14) Variation of reflected power around vehicles is not enough to cause instability in vehicle detection.

(15) Surface reflection coefficients should be devised to be less than 0.1 to be effective for countermeasure, preferably be similar to that of the background environment.

(16) The vehicle detectability is also dependent on background radiation conditions. Night-time ranging enhances range and detectability. The minimum threshold of detection with current detectors is about 10^{-8} watt.

6. RECOMMENDATIONS OF FUTURE WORK

On the basis of this study, it is recommended that further work be carried out to investigate the manner with which the parameters s, μ, and $\emptyset$ might be manipulated by surface coatings, scattering screens, and surface orientation, respectively, to devise effective passive countermeasures. Since this report emphasizes the effect of ranging with laser designations as a special case of ranging, further analytical study on designating is also recommended. Specifically, it is recommended that the following field of work be continued in the next phase:

1. Analysis of range and orientational vulnerability to designators, using equations developed in this report.
2. Numerical computation of designating power, angle of incidence, angle of interception, range, and angle of elevation.
3. Choice and analysis of potential effects of countermeasure coatings.
4. Preparation of coatings for lab experimental evaluation of reflectivity and suitability.

In subsequent phases, the following field of work may be carried out:

1. Consideration of μ and $\emptyset$ for countermeasures by ways of scattering screens and surface orientations.
2. Investigation of reflection characteristics of chosen surface coatings, screens, orientations, and of the actual vehicles by using a practical laser designator such as Nd/yag in the 1.06 micron spectral region.

The greatest present threat to vehicles comes from rangers and designators in the 0.8 to 1.06 micron spectral region. It is conceivable to devise coatings, highly absorbing and lowly reflective, to counter lasers in this spectral region, but such counter may produce a good constrast to background or may produce a good absorber of short-wavelength energies along with a good emitter in the infrared. Further, the advent of multi-color lasers (dye type) would render the "discrete" spectral countering ineffective. It seems that coatings with low reflectivities over a wide spectral region and which would blend with the background are the most desirable. Some suggestions of coatings to be considered are:

(a) Chlorophyll-incorporated paint having reflectivity similar to and blend with that of the background. Chlorophyll may be incorporated by microencapsulation.

(b) Black chrome having a very low reflectivity in the 1 micron region to address the specific threat of the 1.06 micron lasers.

(c) Multilayers of sprayed plastic films selectively applied to address a given background scenario.

The evaluative studies of surface coatings should include specular reflectivity, applicability, reliability, toxicity, blendability, and alterability.

7. APPENDICES

Appendix A.1

Table A.1. Materials parameters for an InSb photovoltaic detector

Parameters	Values (approximate)
V_o, contact potential at 77°K	0.230 eV
N_p, acceptor concentration in the p region	$10^{17}/cm^3$
N_n, donor concentration in the n region	$2.8 \times 10^{16}/cm^3$
n_i, intrinsic concentration at 77°K	$1.6 \times 10^{9}/cm^3$
μ_n, electron mobility at 77°K	1.8×10^{4} $cm^2/v\text{-}s$
μ_p, hole mobility at 77°K	1×10^{3} $cm^2/v\text{-}s$
D_n, electron diffusion coefficient at 77°K	1.2×10^{2} cm^2/sec
D_p, hole diffusion coefficient at 77°K	6.6 cm^2/sec
τ_n, electron lifetime at 77°K	10^{-2} sec
τ_p, hole lifetime at 77°K	10^{-3} sec
L_n, electron diffusion length at 77°K	1.1 cm cm
L_p, hole diffusion length at 77°K	8×10^{-2} cm
D^*_λ, peak detectivity at 77°K and at 5.3 μ	4×10^{11} $\frac{cm\ Hz^{1/2}}{watt}$
α, absorption coefficient at about 5.3 μ	3×10^{4} /cm
E_g, band gap at 77°K	0.230 eV
M_{de}, electron density-state effective mass	0.013 m_o
M_{dh}, hole density-state effective mass	0.318 m_o
ε_r, dielectric constant	17.9

Appendix A. 2

Saturation of InSb Detector:

Estimate of laser power required to saturate InSb photovoltaic detector at 5.3 micron spectral range is made as follows.

High photon flux causes a decrease in potential barrier ($V_o - V_f$), where V_o is the contact potential of the p-n junction and V_f is the photovoltage generated by absorption of photon in the barrier region. The photon flux density per second is related to V_o, V_f, and the materials parameters (given in Table A.1) as follows:

$$\phi = A_o \left[\exp\left(\frac{q\ V_t}{KT}\right) - 1\right] \left[V_o - V_f\right]^{-1/2}, \text{ where}$$

$$A_o = \left[\frac{1}{2}\right] \left[\frac{q\ N_p\ N_n}{2\varepsilon_r (N_p\ N_n)}\right]^{1/2} \left[\frac{n_i^2}{N_p\ N_n}\right] \left[\frac{D_p\ N_p}{L_p} + \frac{D_n\ N_n}{L_n}\right]$$

$$= 5.8 \times 10^3 \left(\frac{\text{photon-V}^{1/2}}{\text{sec-cm}^2}\right)$$

Assume saturation begins when V_f reaches 90% of the V_o value, i.e. when $V_f = 0.207$ V. The photon flux density (ϕ) required for saturation is then:

$$\phi = (5.8 \times 10^3) \frac{\left[\exp\left(\frac{q\ 0.207}{KT}\right) - 1\right]}{(0.230 - 0.207)^{1/2}}$$

$$= 1.3 \times 10^{18} \text{ photon/sec/cm}^2$$

At $\lambda = 5.3 \times 10^{-4}$ cm, the energy per photon is 3.75×10^{-20} joules. Then, the irradiance (H_S) required for saturation is given by

$$H_S = \phi \left(\frac{hc}{\lambda}\right)$$
$$= 4.9 \times 10^{-2} \text{ watt/cm}^2$$

If the laser required to saturate the InSb detector has power P, range 5×10^4 cm, and divergence 1×10^{-3} radian, then P is estimated to be:

$$P = H_S \times \text{beam area} = 96 \text{ watts}$$

The above analysis neglects several factors including atmospheric condition, surface reflectivity, beam-area distribution, and collimating optical effects. A more detailed analysis of saturation of photovoltage and photocurrent in p-n junctions has been presented by Dhariwal et al.[34]

P_r = reflected power received by receiver

$$= J_r \left(\frac{A_o}{R_r^2}\right) \quad T_o \quad e^{-\mu_r R_r} \qquad \text{(watt)}$$

$$= \frac{4s\ P_T\ A_{T1}\ A_o\ T_o \cos \phi_t \ \cos \phi_r\, e^{-\mu_t R_t} e^{-\mu_r R_r}}{\pi^2 \theta^2 R_t^2 R_r^2} \quad \text{(watt)} \qquad (1)$$

Equation (1) may be expressed in the following generic terms:

$$P_r = P_T\,[4/(\pi\theta^2)]\,[A_o T_o]\left[\frac{s\,A_{T1}\cos\phi_t\cos\phi_r}{\pi R_t^2 R_r^2}\right][e^{-\mu_t R_t}][e^{-\mu_r R_r}]$$

$$\equiv P_T[F_t]\,[F_r]\,[F(\phi_t, \theta_r)]\,[A_t]\,[A_r]$$

where

F_t = optical function of the laser transmitter

F_r = optical function of the receiver

$F(\phi_t, \phi_r)$ = scattering function of the surface

A_t = atmospheric function of the transmitted beam

A_r = atmospheric function of the reflected beam

Equation (1) assumes a rectangular power distribution of the laser beam, such that the divergence is defined by the width of the rectangular distribution, as shown in Fig. 1A.

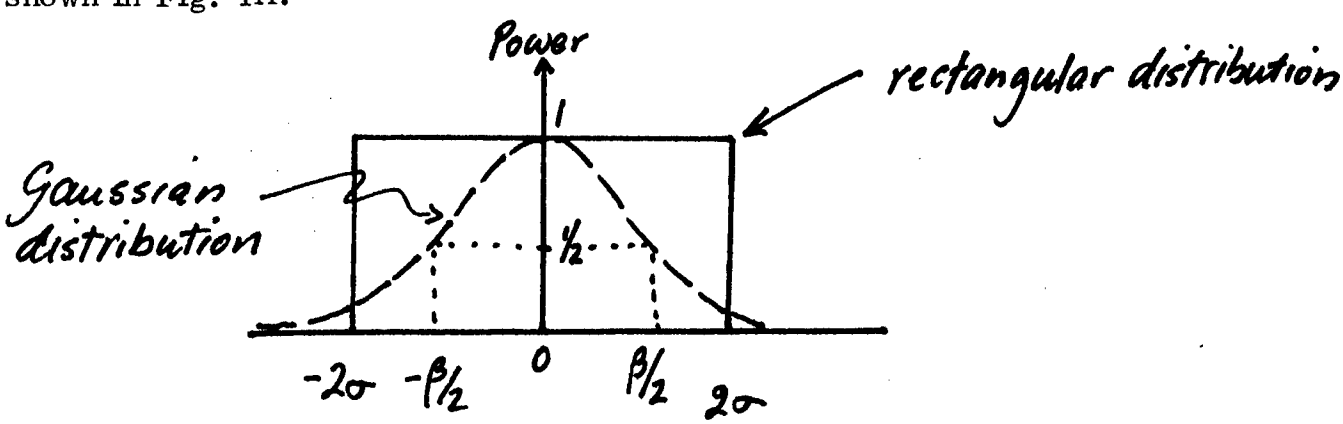

Fig. 1A. Relationship between Gaussian and rectangular distribution.

For the rectangular distribution, the divergence θ is 4σ. If the divergence for the Gaussian distribution is β, then $\theta \simeq 1.7\beta$.

Equation (1) is applicable to rangers as well as designators, and if a camouflage scattering screen is deployed about the surface, then (1) becomes

$$P_r = \frac{4s\ P_T A_{T1}\ A_o\ T_o \cos \phi_t \cos \phi_r\ e^{-\mu_t R_t}\ e^{-\mu_r R_r}\ e^{-2\mu_x R_x}}{\pi^2 \theta^2 R_t^2 R_r^2} \qquad (2)$$

where

μ_x = extinction coefficient

R_x = thickness of screen

$\ll R_t, R_r$

Case 2: For a ranger ranging an infinite, diffused surface

The reflected power may be simplied to

$$P_r = \frac{P_T\ A_o\ T_o\ s\ (\cos \phi_t)\ e^{-2\mu R}}{\pi R^2} \qquad (3)$$

or

$$= \frac{P_T\ T_o\ s\ (\cos \phi_t)\ D^2\ e^{-2\mu R}}{4R^2} \qquad (4)$$

where $R = R_t = R_r$

$\mu = \mu_r = \mu_t$

$R_x = 0$

D = diameter of the optics

Case 3: For rangers ranging a finite, diffused surface

The reflected power becomes

$$P_r = \frac{4\ s\ P_T\ A_o\ A_S\ T_o\ (\cos^2 \phi_t)\ e^{-2\mu R}}{\pi^2 \theta^2 R^4} \qquad (5)$$

where $A_{T1} = A_S \ll A_b$

$R_x = 0$

Case 4: For rangers ranging a retroreflective surface

If the diameter of the receiver optics is large enough to intercept totally the retroreflected beam, then the reflected power is:

$$P_r = \frac{4 P_T T_o s A_s \cos \phi_t}{\pi R^2 \theta^2} \qquad (6)$$

If the diameter of the receiver optics is smaller than the retroreflected beam, then the reflected power is

$$P_r = \frac{4 P_T T_o s D^2 A_s \cos \phi_t}{\pi R^4 \theta^2 \bar{\gamma}^2} \qquad (7)$$

where $\bar{\gamma}$ = effective reflected beam divergence. An approximate method of obtaining a specific form of equation (7) may be given as below:

Consider the Gaussian distribution of the laser beam cross section to be approximately cosine distribution as shown in Fig. 2A.

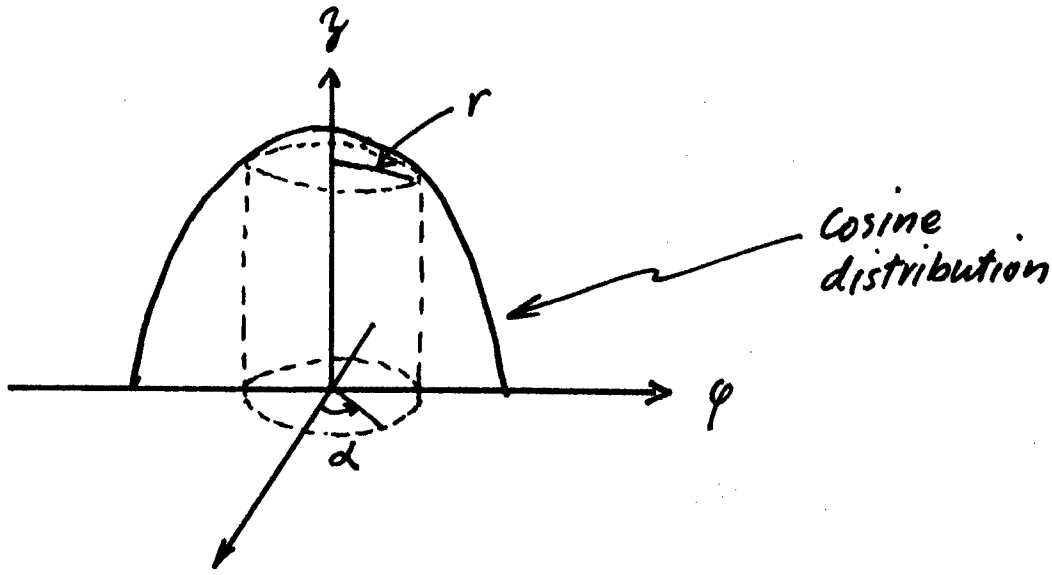

Fig. 2A. Cosine approximation of the Gaussian distribution (the cylindrical coordinates: z, r, and α are used to obtain volume under the cosine envelope.)

An elemental volume under the cosine envelope in cylindrical coordinates:

$$dV = (r\, d\alpha)\, dz\, dr$$

The total volume (V) under the cosine envelope:

$$A(V) = A \int_{\alpha=0}^{\alpha=2\pi} \int_{r=0}^{r=\varphi} \int_{z=0}^{z=\cos r} dz\, (r\, dr)\, d\alpha$$

$$= 2\pi A\, [\cos\varphi + \varphi \sin\varphi - 1] \qquad (8)$$

where A is chosen so that AV = 1 when $\varphi = \frac{\pi}{2}$.

When $\varphi = \frac{\pi}{2}$, $2\pi A\, [\cos(\frac{\pi}{2}) + \frac{\pi}{2} \sin(\frac{\pi}{2}) - 1] = 1$

So $A = (\frac{1}{2\pi})(\frac{1}{0.5708})$

$$= \underline{0.279} \qquad (9)$$

The relationship between φ and divergence θ may be obtained by considering Fig. 3A.

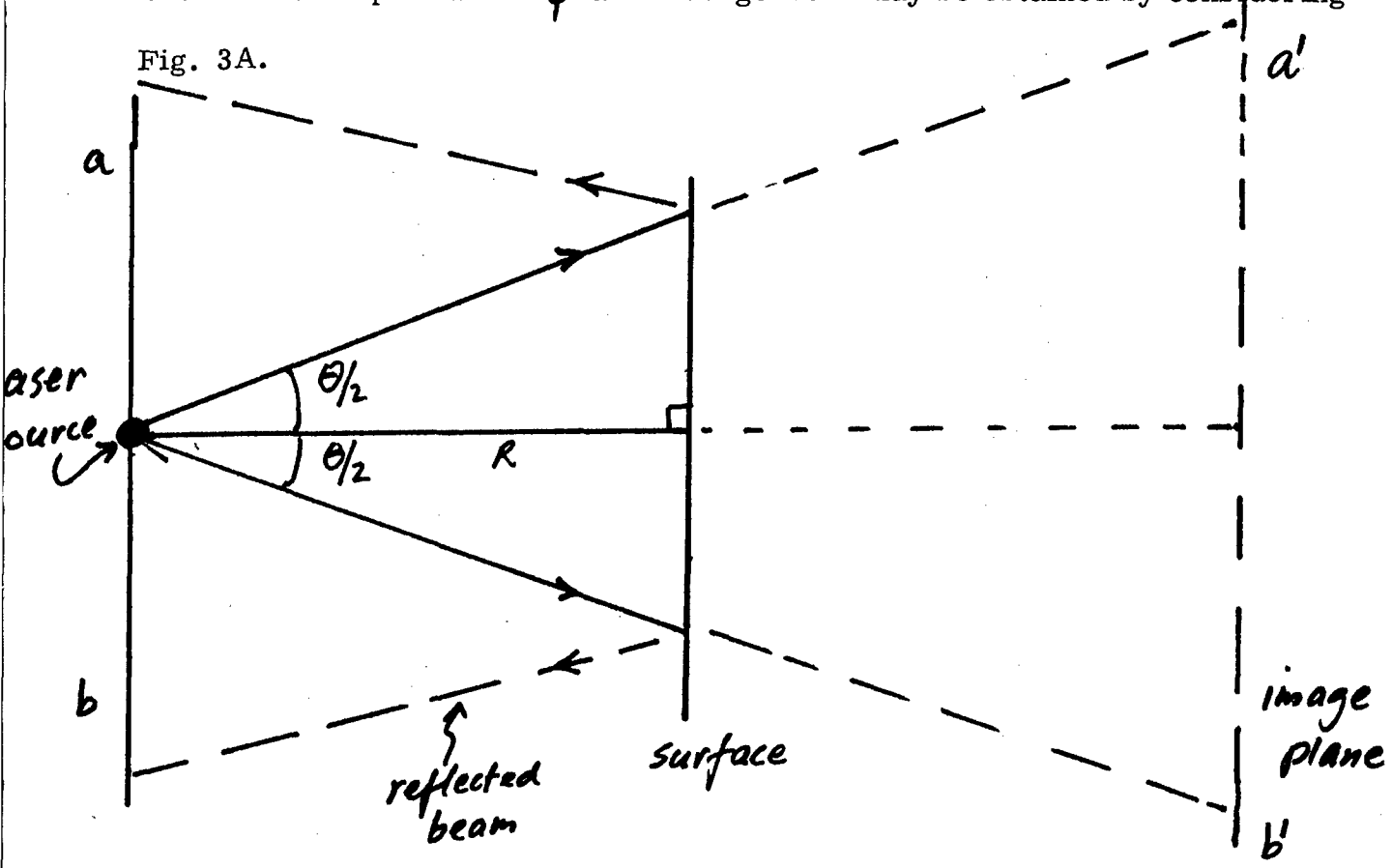

Fig 3A: Reflection geometry in obtaining a relation between φ and θ.

Referring to Fig. 3A, a'b' is the image plane of the plane intercepting the reflected beam at the receiver. If θ is the beam divergence, then the beam radius r_b at ab is related to θ:

$$\frac{\theta}{2} = \frac{r_b}{2R}$$

The radius r_b corresponds to $(\pi/2)$ of the cosine distribution, as r_o corresponds to φ, then

$$\frac{\pi/2}{r_b} = \frac{\varphi}{r_o} \qquad \text{(by the similarity principle)}$$

i.e. $$\frac{(\pi/2)}{(\theta/2)\,2R} = \frac{\varphi}{r_o}$$

$$\varphi = \left(\frac{\pi\, r_o}{2\theta\, R}\right) \tag{10}$$

Now, if r_o is the radius of the receiver optics, so the reflected power received by the optics is

$$P_r = P_T\, T_o\, s\, [A \times 2 \times \pi\, (\cos\varphi + \varphi \sin\varphi - 1)] \cos\gamma\, e^{-2\mu R}$$

where $$\varphi = \frac{\pi r_o}{2\theta R} \tag{11}$$

and $$\gamma = \left(\frac{\pi}{2}\,\frac{\phi}{\theta/2}\right)$$

It is noted that, for a reflecting surface, the optics can receive only a fraction of the total reflected power, and only when the angle of incidence (ϕ) is smaller than the half divergence angle ($\theta/2$); otherwise, no reflected power is received at all.

Case 5: For rangers ranging a multi-surface target

If there are n surfaces being irradiated by the ranger laser beam and the ith surface is represented by a set of condition (A_{si}, s_i, ϕ_i, m_i), then the total reflected power received by the receiver optics is the sum of the reflected powers from the different surfaces. For this case, which is applicable to any vehicle surface, we assume a worst-case analysis such that the enemy's laser beam is aimed onto the highest reflecting surface, and if that surface did not fill the beam area, the beam can aim and add part (or all) of the second most reflecting surface, etc., adding more surfaces (as needed) until either the entire beam area is filled, or until all the visible vehicle surfaces are added. The reflecting condition of a given surface may be described by a modifying factor m which is used to compensate for effects of cluttering etc.; m is usually about unity but can vary $0 \leq m \leq \sec \phi$. Using this factor m, the n surfaces may be tested for visibility, and then ordered into a priority scheme with the surface (A_{s1}, s_1, ϕ_1, m_1) being the most visible. Normally, closely ranked surfaces are physically adjacent to one another.

If the beam area is less than the projected area of the entire target of n visible surfaces, the reflected power received by the optics may be expressed as (with the aid of equation (5)):

$$P_r = \left(\frac{4 P_T A_o T_o e^{-2\mu R}}{\pi^2 R^4 \theta^2} \right) \left[\sum_{i=1}^{i=n-1} (s_i m_i A_i \cos^2 \phi_i) + s_n m_n \cos \phi_n \left(A_b - \sum_{y=1}^{n-1} A_y \cos \phi_y \right. \right. \quad (12)$$

If the beam area exceeds the projected area of the target of n surfaces,

then equation (12) reduces to:

$$P_r = \left(\frac{4\ P_T\ A_o\ T_o\ e^{-2\mu R}}{\pi^2\ R^4\ \theta^2} \right) \left[\sum_{i=1}^{n} s_i\ m_i\ A_i \cos^2 \phi_i \right] \qquad (13)$$

REFERENCES

1. S. Fine et al. Fed. Proc. 24 (1), Suppl. 14 S-35 (1965)

2. J. F. Carr, Lasers in Industry, Edited by S. S. Charschan, Chapter 10, 579, Van Nostrand Reinhold, N.Y. (1972)

3. L. Goldman, Ann. N.Y. Acad. Sci. 122, 802 (1965)

4. L. Goldman, J. Am. Med. Assoc. 180, 302 (1964)

5. John F. Ready, Effects of High-Power Laser Radiation, Acad. Press, N.Y. (1971)

6. F. P. Gagliano and V. J. Zaleckas, Lasers in Industry, Edited by S. S. Charchan, Chapter 3, 139, Van Nostrand Reinhold, N.Y. (1972)

7. F. W. Dabby and U. C. Pack, IEEE J. Quant. Electronics, QE-8, 106 (1972)

8. John F. Ready, Effects of High-Power Laser Radiation, Chapter 3, 67, Acad. Press, N.Y. (1971)

9. H. G. Landau, Quart. J. Appl. Math. 8, 81, (1950)

10. A. M. Bouch-Bruevich et al. Sov. Phys.-Tech. Phys. 13, 640 (1968)

11. C. M. Percival, J. Appl. Phys. 38, 5313 (1967)

12. P. W. Kruse et al. Elements of Infrared Technology, Wiley & Sons, N.Y. (1968)

13. J. F. Ready, Effects of High-Power Laser Radiation, Chapter 6, 277, Acad. Press, N.Y. (1971)

14. C. A. Pitha, Air Force Cambridge Res. Lab. Rep. No. 67-0317 (1967)

15. A. Yariv, Quantum Electronics, Chapter 25, Wiley, N.Y. (1967)

16. R. Y. Chiao, et al. Phys. Rev. Lett. 12, 592 (1964)

17. T. P. Belikova, et al. Sov. Phys. JETP 27, 19 (1968)

18. V. I. Vladimirov, et al. Sov. Phys. - Solid State 9, 411 (1967)

19. J. H. Cullom and R. W. Waynant, Appl. Opt. 3, 989 (1964)

20. A. A. Grinberg et al. Sov. Phys. - Solid State 9, 1085 (1967)

21. M. Bertolotti et al. J. Appl. Phys. 38, 4088 (1967)

22. M. Kruer et al. Opt. and Quant. Elect. 8, 453 (1976)

23. M. Birnbaum, et al. Appl. Phys. Lett. 10, 227 (1967)

24. C. R. Hammond and C. R. Stanley, Opto-Electronics, 5, 249 (1973)

25. T. S. Moss, G. L. Burrell, and B. Ellis, Semiconductor Opto-Electronics, Butterworths, London (1973)

26. J. Bardeen, Bell System Tech. J. 29, 469 (1950)

27. Yoshiharu Matsuoka and Akira Usami, Opto-Electronics 6, 217 (1974)

28. M. L. Stitch, Laser Handbook 2, Chapter F7, 1745 (1972); North-Holland, Amsterdam

29. Walter Koechner, IEEE-AES, 4, 81 (1968)

30. Eugene R. Leach, et al. U. S. Army Equipment Research and Development Center, Fort Belvoir, Virginia, Report CTR-18 (1974)

31. L. Mandel, Proc. Phys. Soc. 74, 233 (1959)

32. F. J. Myers, Infrared Information Symposium San Francisco, 6, 103 (1961)

33. H. Kanbe, et al., Electron Devices, IEEE, 23, 1337 (1976)

34. S. R. Dhariwal, et al. Electron Devices, IEEE, 23, 504 (1976)

35. Handbook of Lasers, Editor Robert J. Pressley, CRC Press, Ohio (1971)

*

FIG. 1(a)
VARIOUS VIEWS OF M48A1

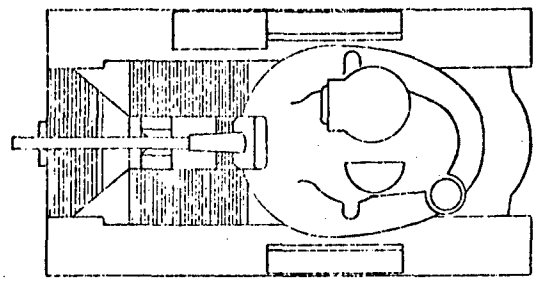

TOP VIEW

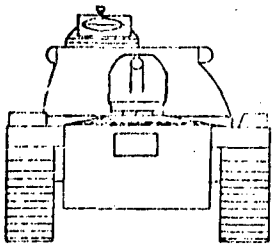

FRONT VIEW

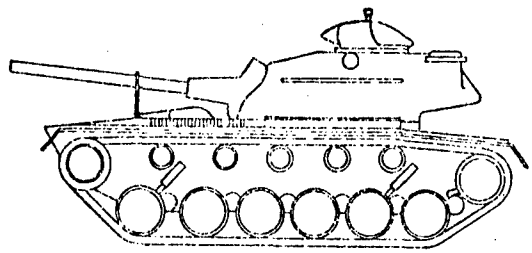

SIDE VIEW (1)

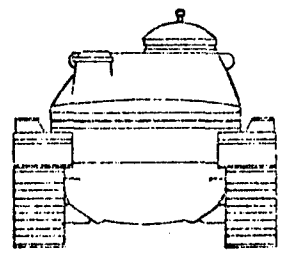

BACK VIEW

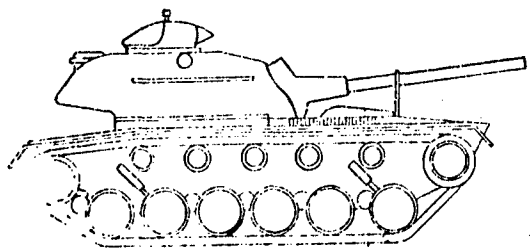

SIDE VIEW (2)

FIG. 1(b)*
VARIOUS VIEWS OF M113APC

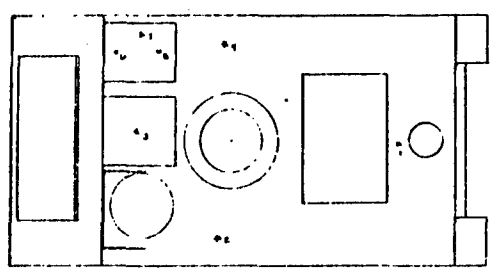

TOP VIEW

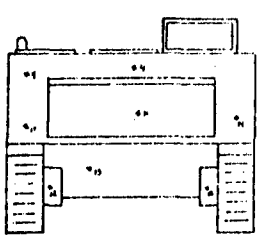

FRONT VIEW

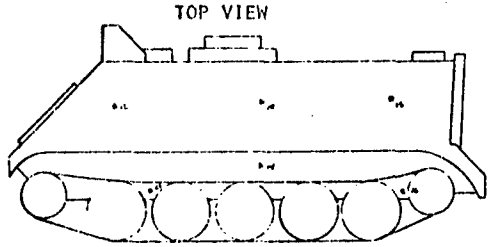

SIDE VIEW (1)

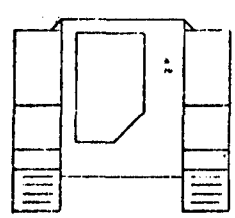

BACK VIEW

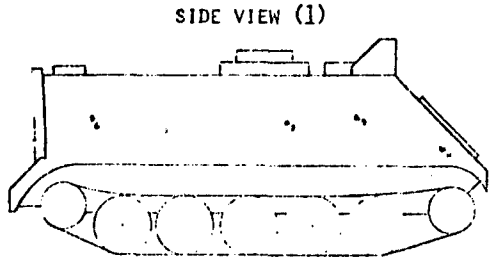

SIDE VIEW (2)

*These figures were drawn by William Reynolds of MTU.

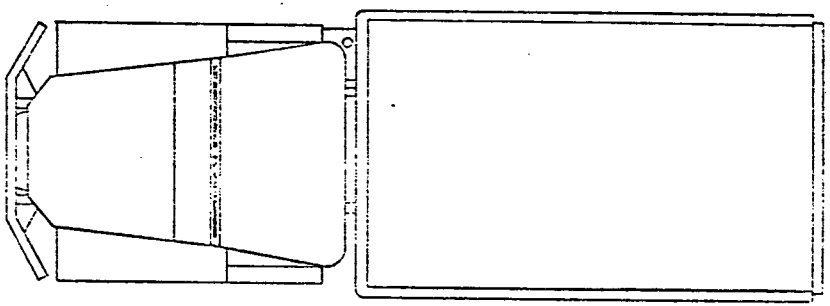

Top View

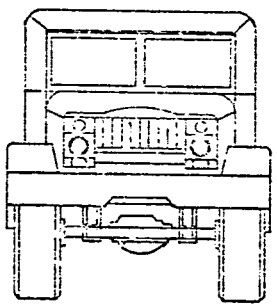

Front View

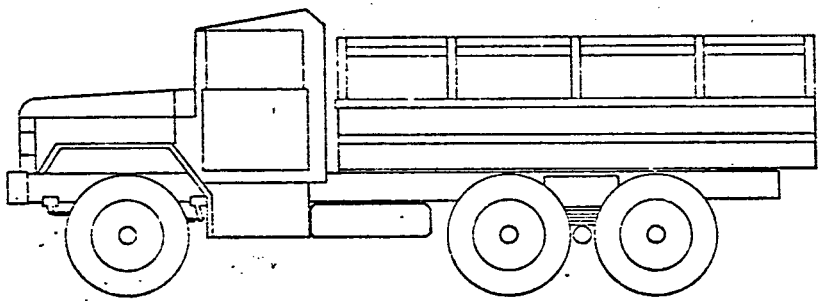

Side View (1)

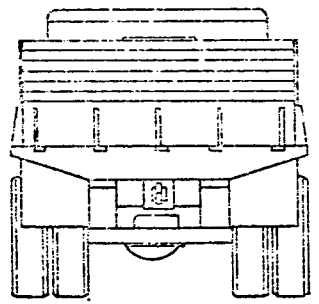

Back View

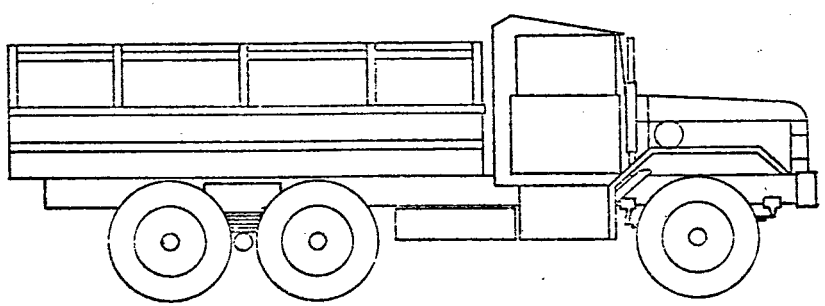

*Fig. 2. Various View of the M35A

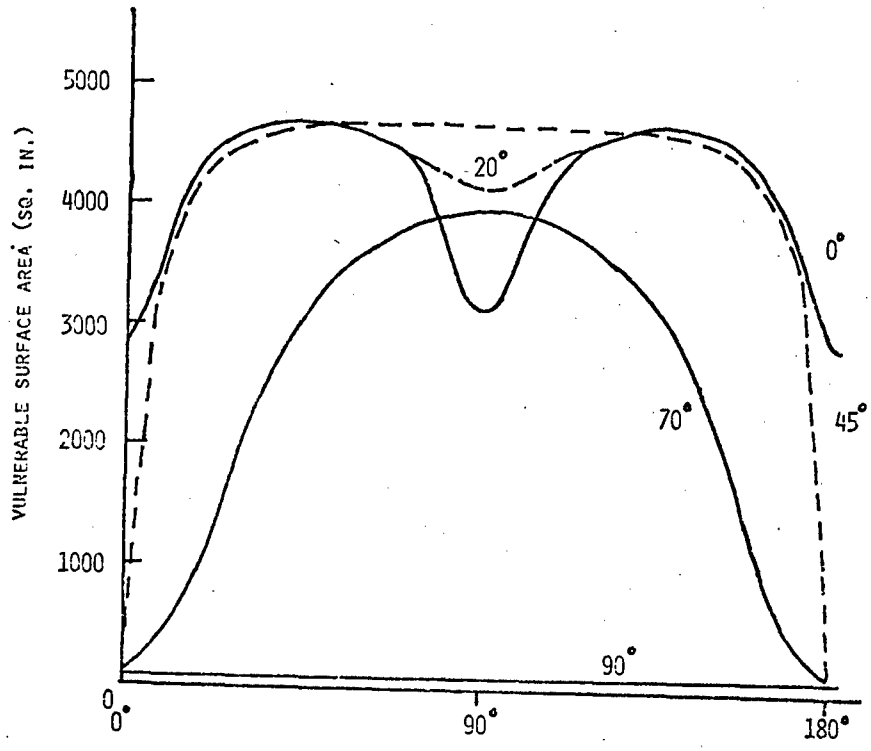

FIG. 3. VULNERABLE SURFACE AREA OF M48A1 VS. ANGLE OF ROTATION AROUND VEHICLE WITH ANGLE OF INCIDENCE AS THE PARAMETER.

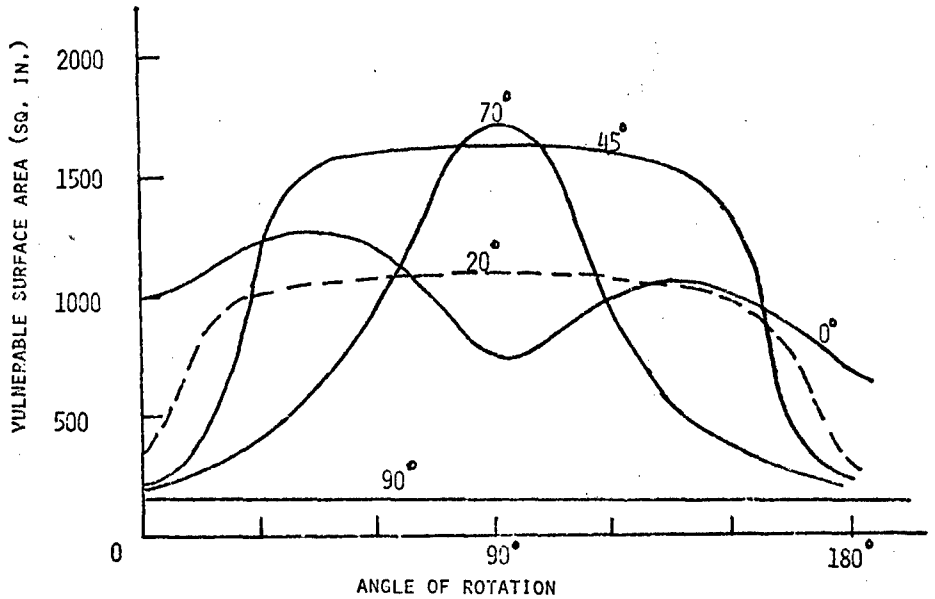

FIG. 4. VULNERABLE SURFACE AREA OF M113 VS. ANGLE OF ROTATION AROUND VEHICLE WITH ANGLE OF INCIDENCE AS THE PARAMETER.

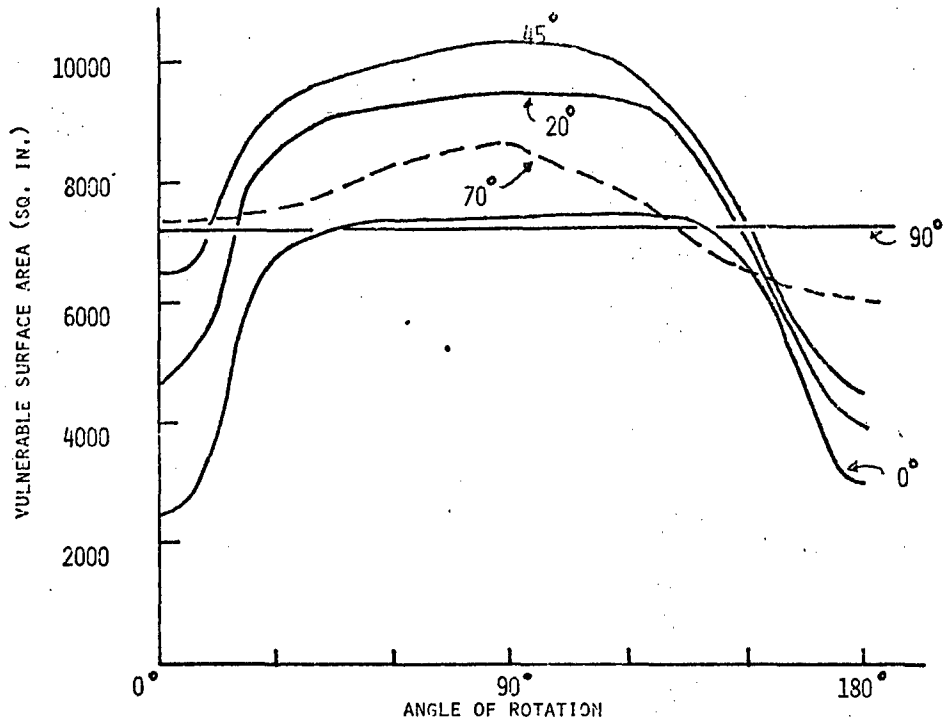

FIG. 5. VULNERABLE SURFACE AREA OF THE M35A TRUCK VS. ANGLE OF ROTATION AROUND VEHICLE WITH ANGLE OF INCIDENCE AS THE PARAMETER.

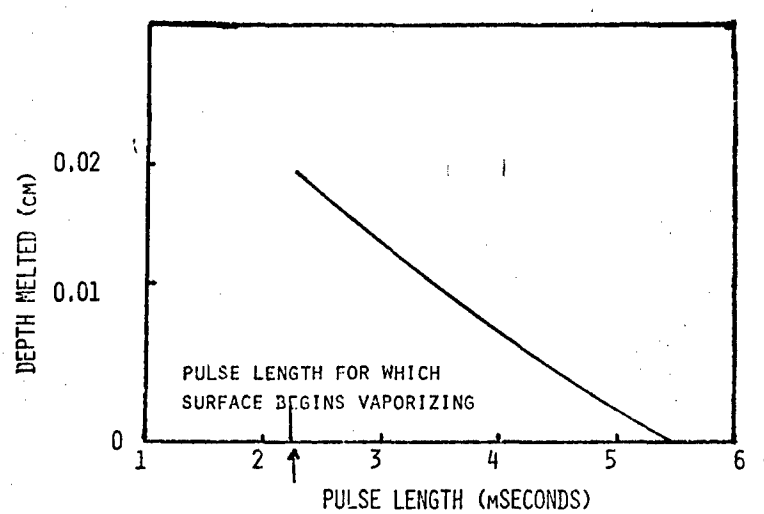

FIGURE 6. CALCULATED DEPTH AT WHICH THE MELTING POINT IS REACHED (IN COPPER) AS A FUNCTION OF PULSE LENGTH.

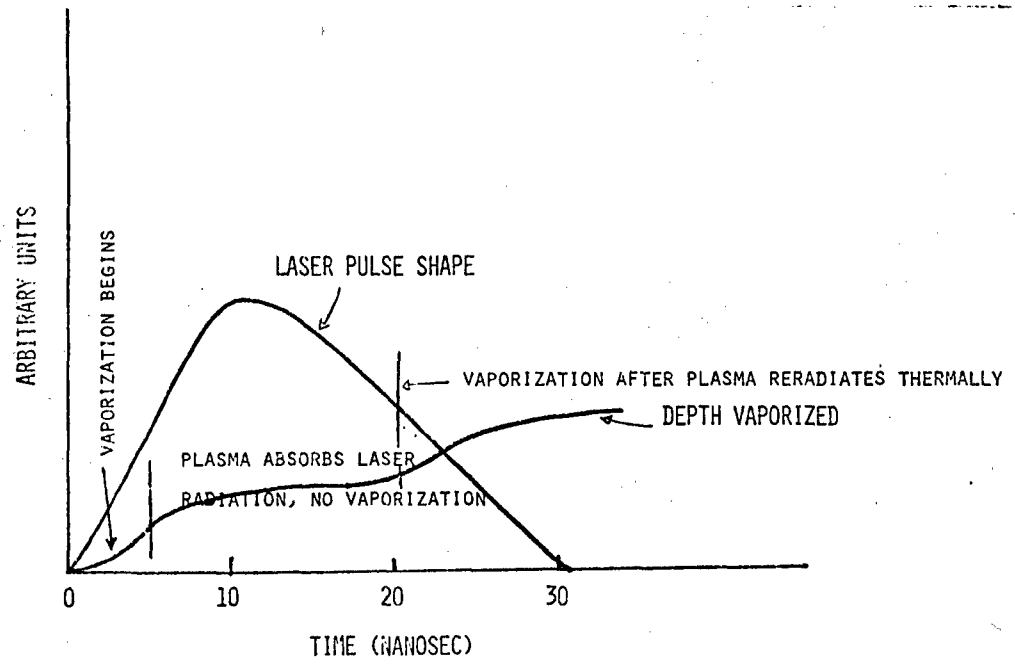

FIGURE 7. SCHEMATIC REPRESENTATION OF THE DEPTH VAPORIZED AS A FUNCTION OF TIME BY A HIGH FLUX DENSITY PULSE.

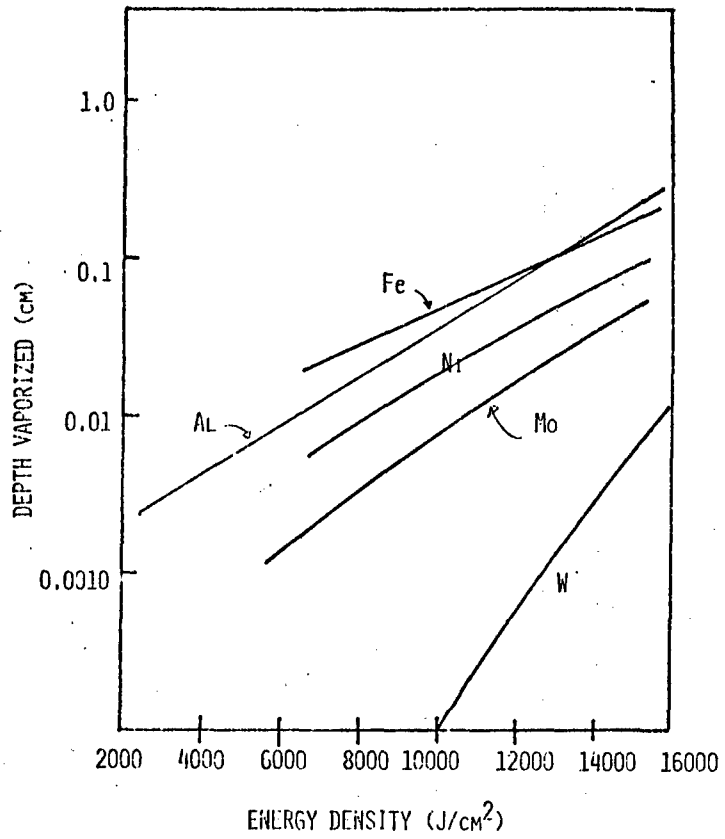

FIGURE 8. EXPERIMENTAL DEPTH VAPORIZED FOR VARIOUS METALS IRRADIATED BY A 700-μSEC LASER PULSE.

Figure 9. Structural representation of an optical or imagery system

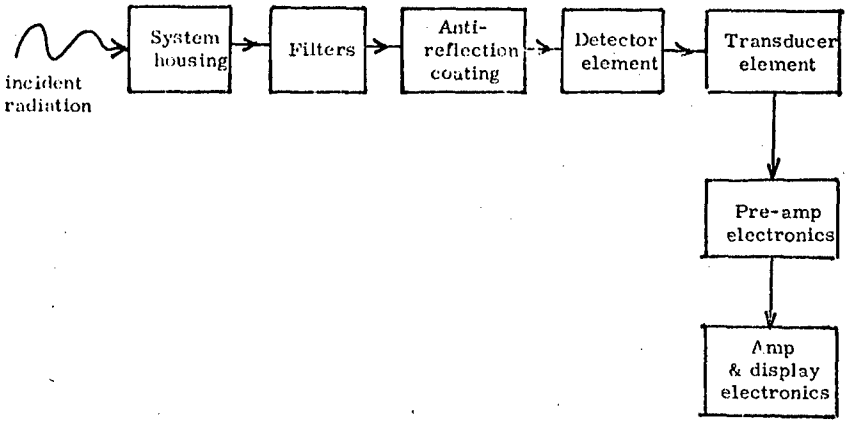

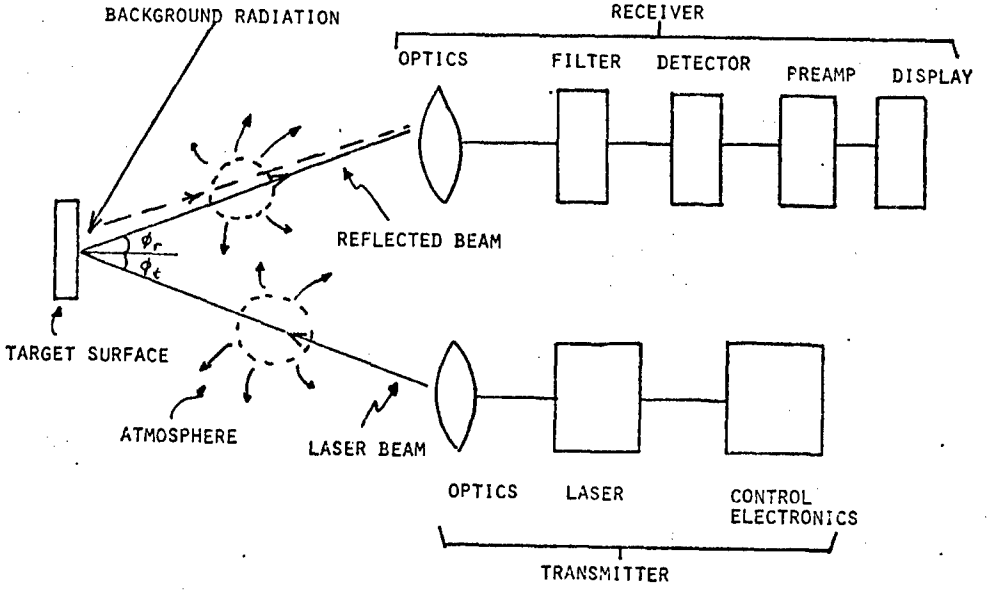

FIG. 10. DISPOSITION OF A RANGER OR A DESIGNATOR RELATIVE TO THE VEHICLE REFLECTING SURFACE.

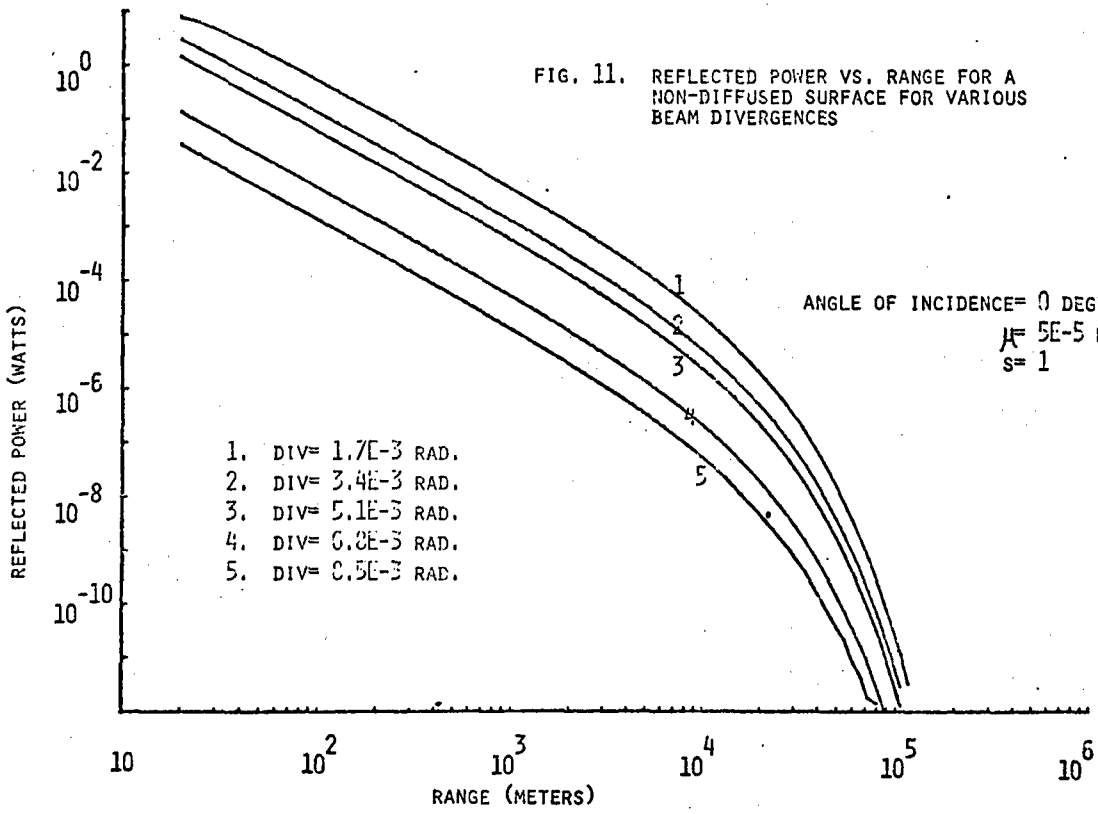

FIG. 11. REFLECTED POWER VS. RANGE FOR A NON-DIFFUSED SURFACE FOR VARIOUS BEAM DIVERGENCES

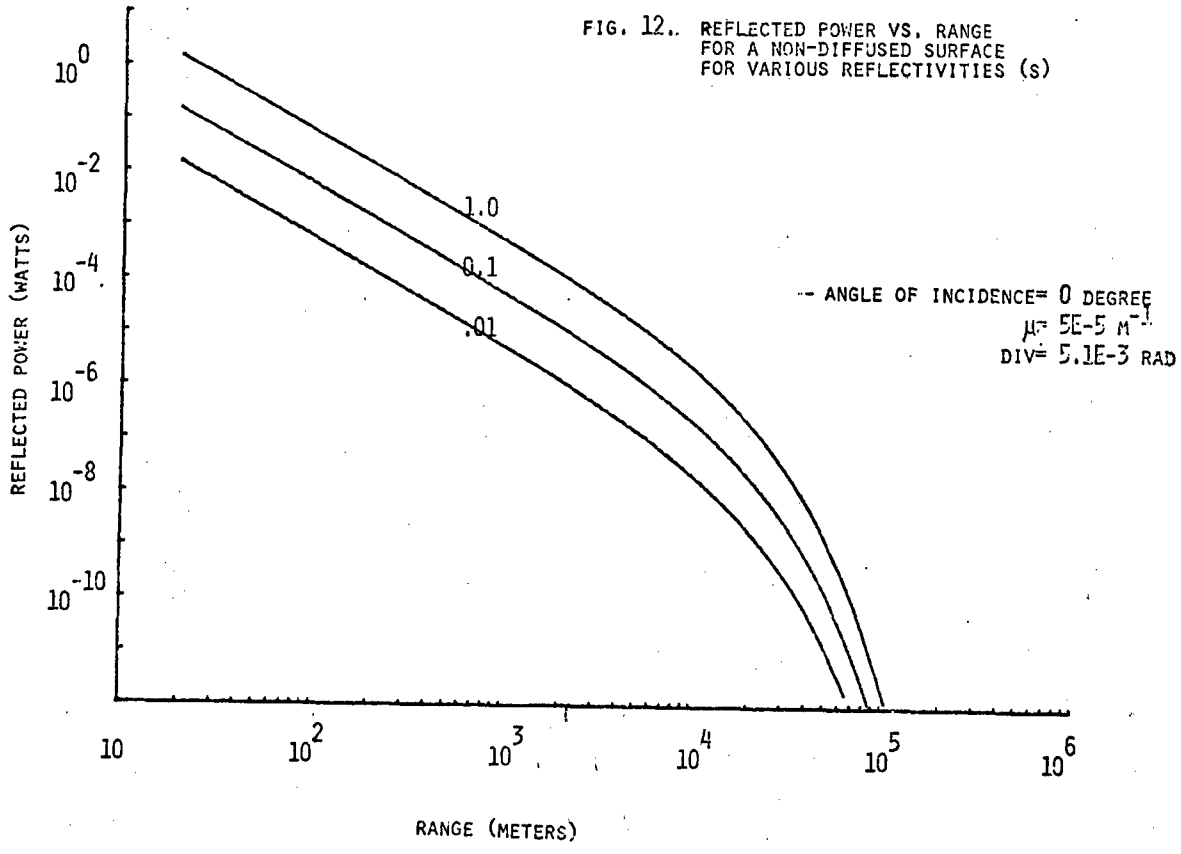

FIG. 12. REFLECTED POWER VS. RANGE FOR A NON-DIFFUSED SURFACE FOR VARIOUS REFLECTIVITIES (s)

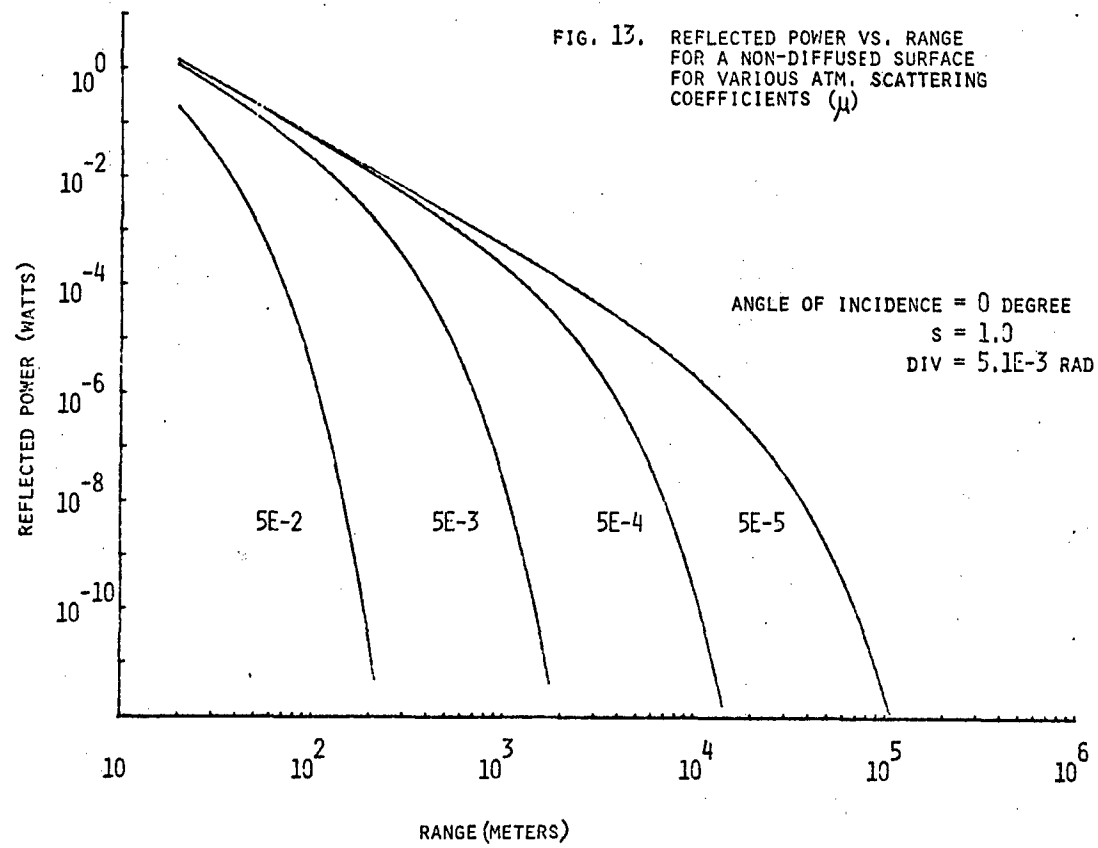

FIG. 13. REFLECTED POWER VS. RANGE FOR A NON-DIFFUSED SURFACE FOR VARIOUS ATM. SCATTERING COEFFICIENTS (μ)

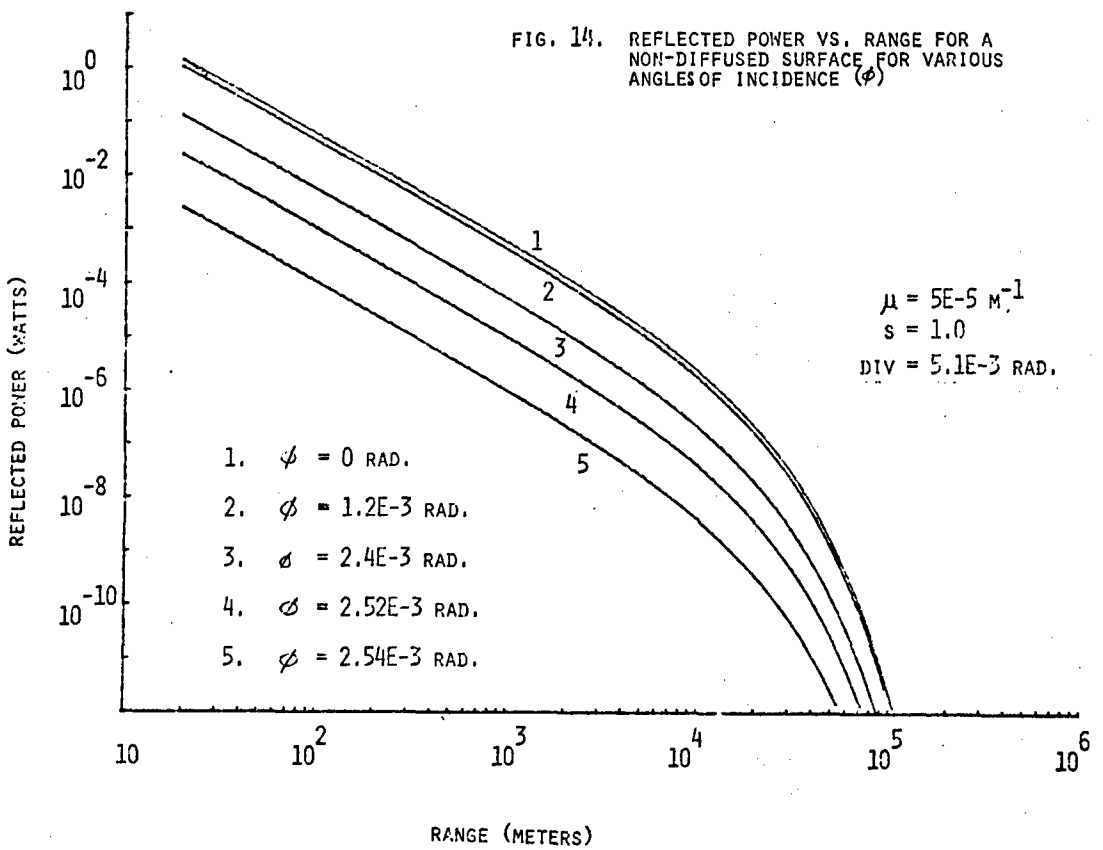

FIG. 14. REFLECTED POWER VS. RANGE FOR A NON-DIFFUSED SURFACE FOR VARIOUS ANGLES OF INCIDENCE (ϕ)

FIG. 15. REFLECTED POWER VS. RANGE FOR A DIFFUSED SURFACE FOR VARIOUS ATMOSPHERIC SCATTERING COEFFICIENTS (μ)

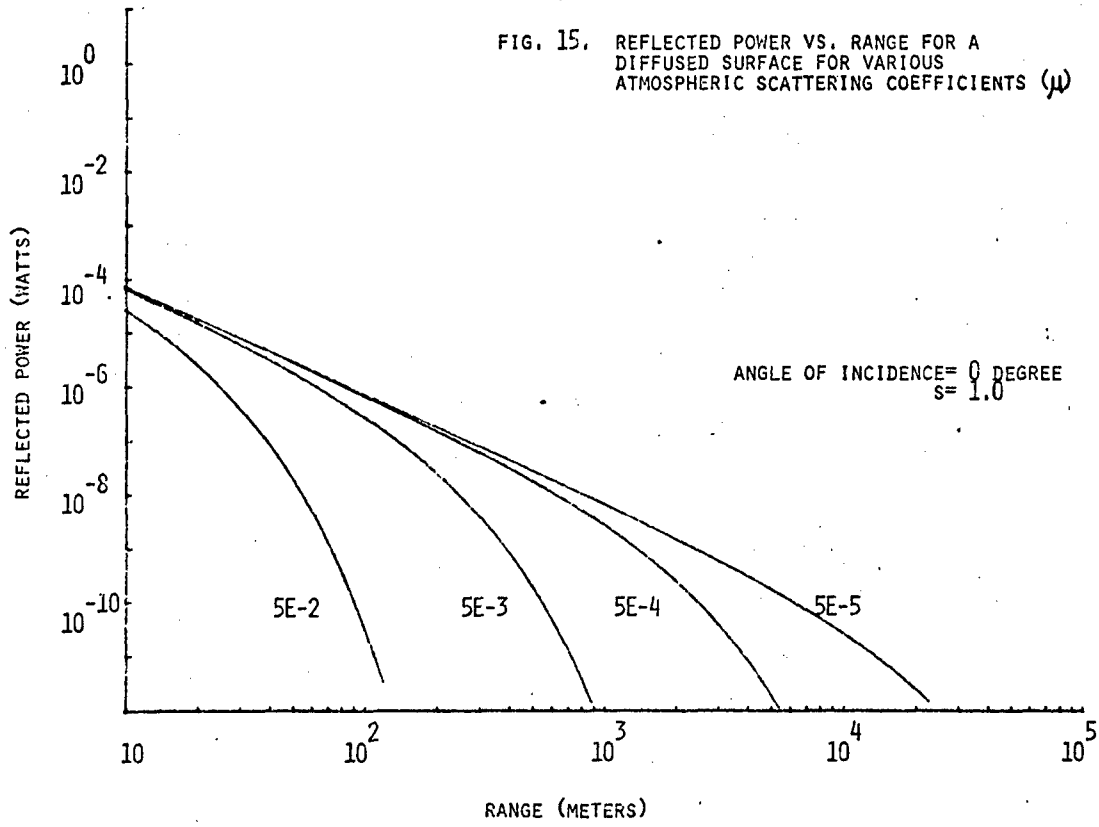

FIG. 16. REFLECTED POWER VS. RANGE FOR A DIFFUSED SURFACE FOR VARIOUS REFLECTIVITIES (s)

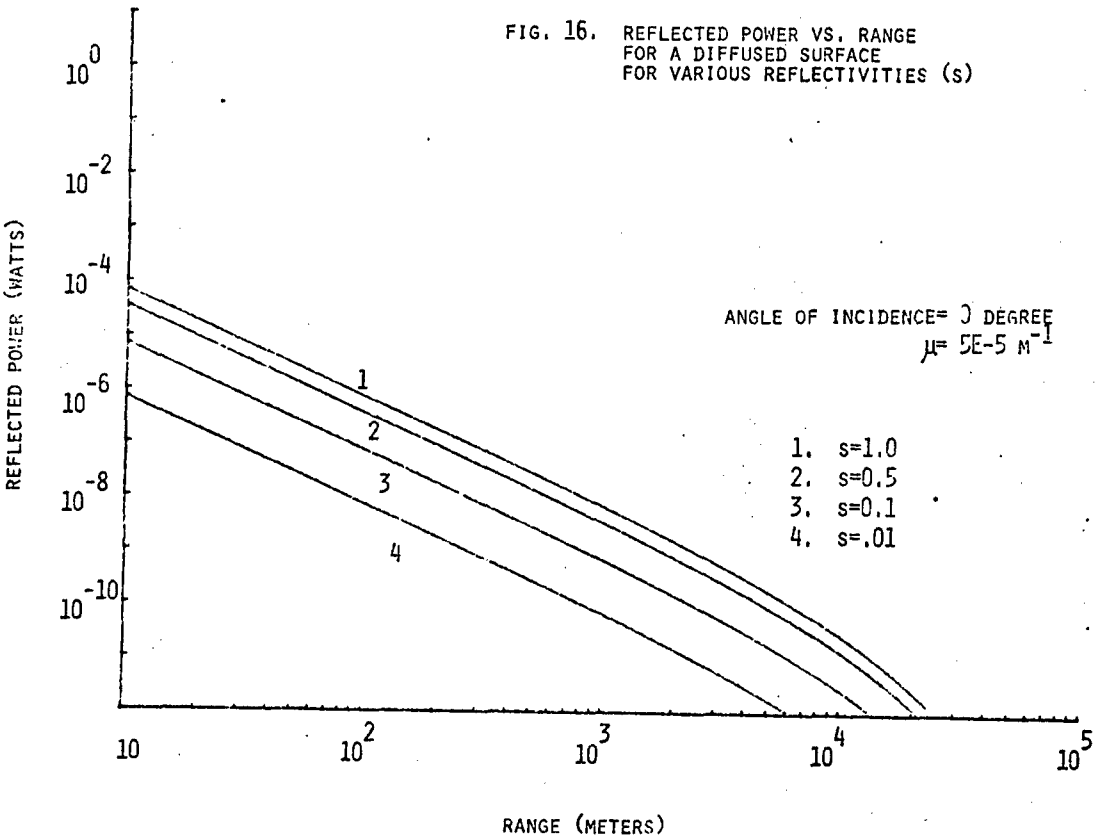

FIG. 17. REFLECTED POWER VS. ANGLE OF ROTATION FOR A DIFFUSED SURFACE FOR VARIOUS ANGLES OF INCIDENCE (Ø)

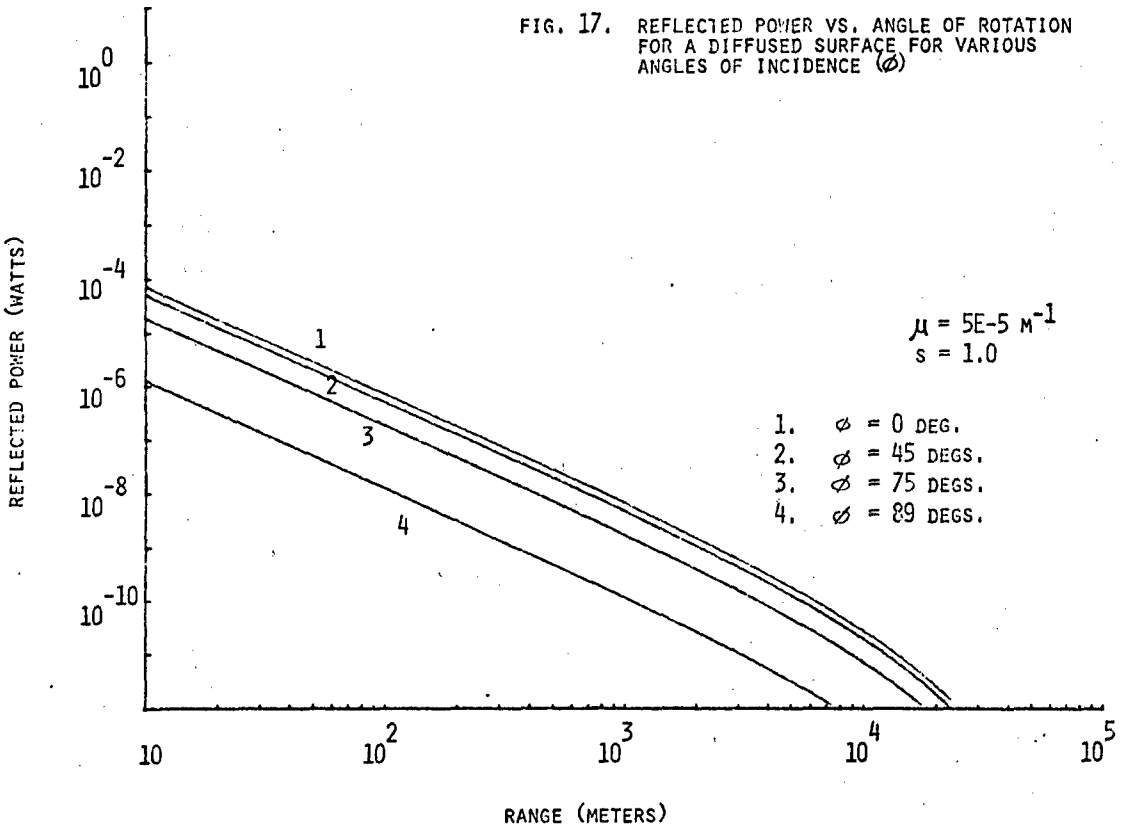

FIG. 18. REFLECTED POWER VS. RANGE FOR A DIFFUSED SURFACE FOR VARIOUS EXTINCTION COEFFICIENTS (μ_x) OF SCATTERING SCREEN

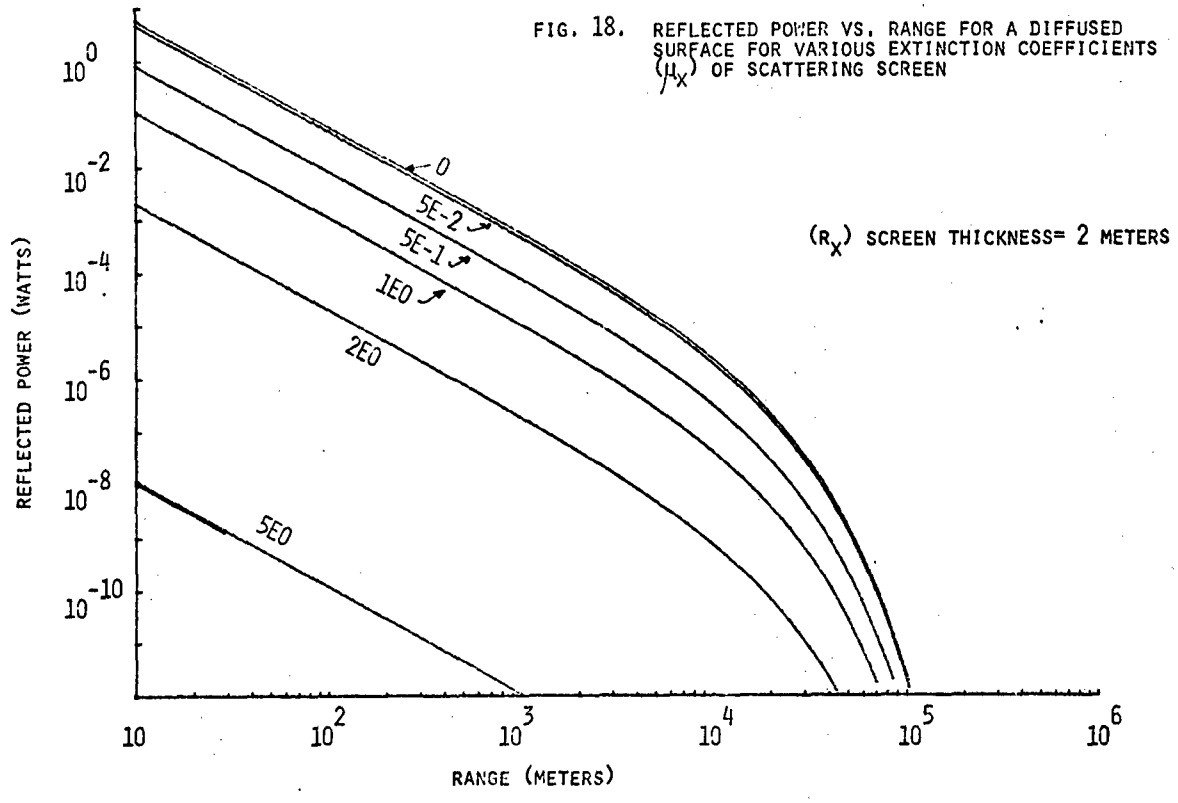

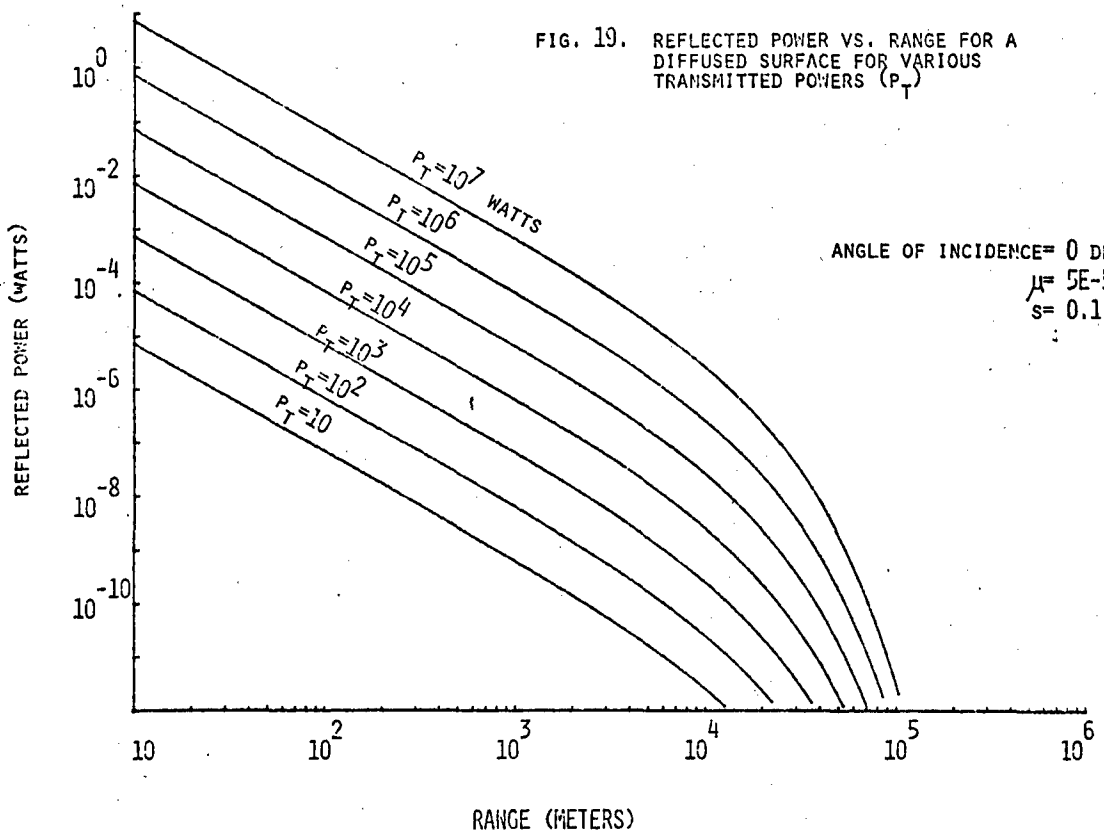

FIG. 19. REFLECTED POWER VS. RANGE FOR A DIFFUSED SURFACE FOR VARIOUS TRANSMITTED POWERS (P_T)

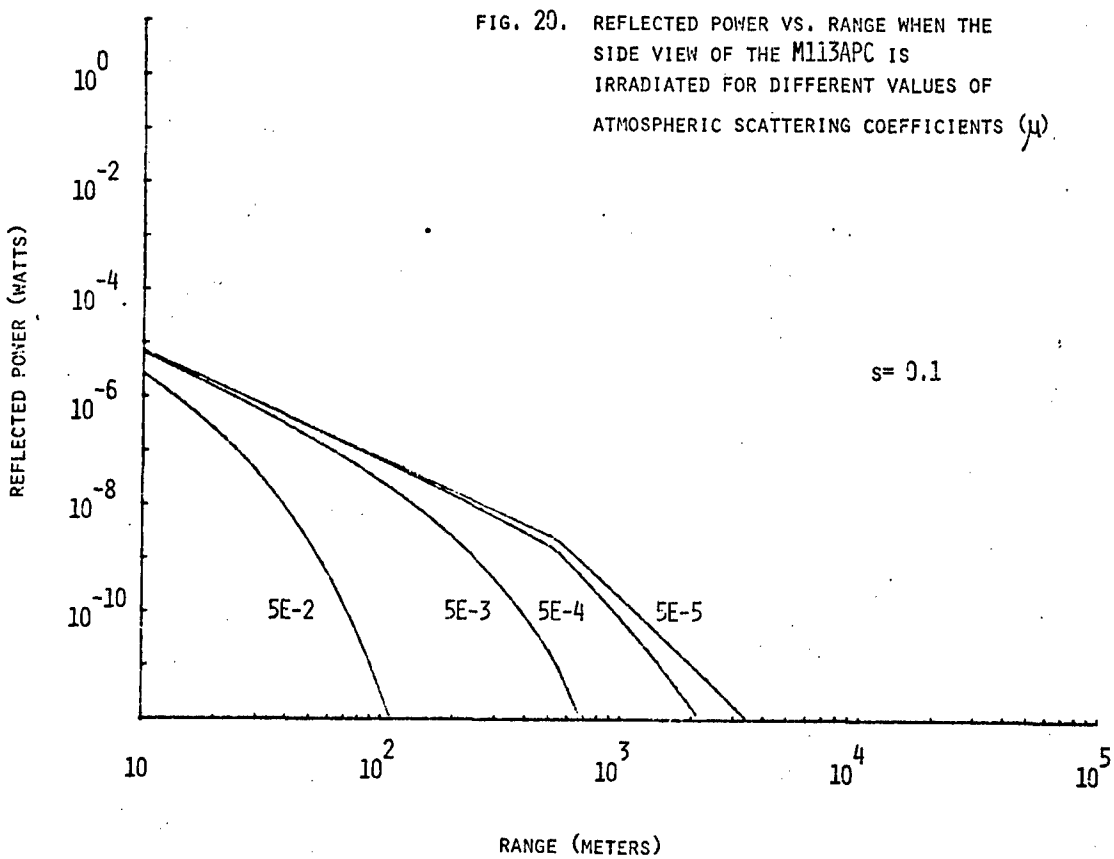

FIG. 20. REFLECTED POWER VS. RANGE WHEN THE SIDE VIEW OF THE M113APC IS IRRADIATED FOR DIFFERENT VALUES OF ATMOSPHERIC SCATTERING COEFFICIENTS (μ)

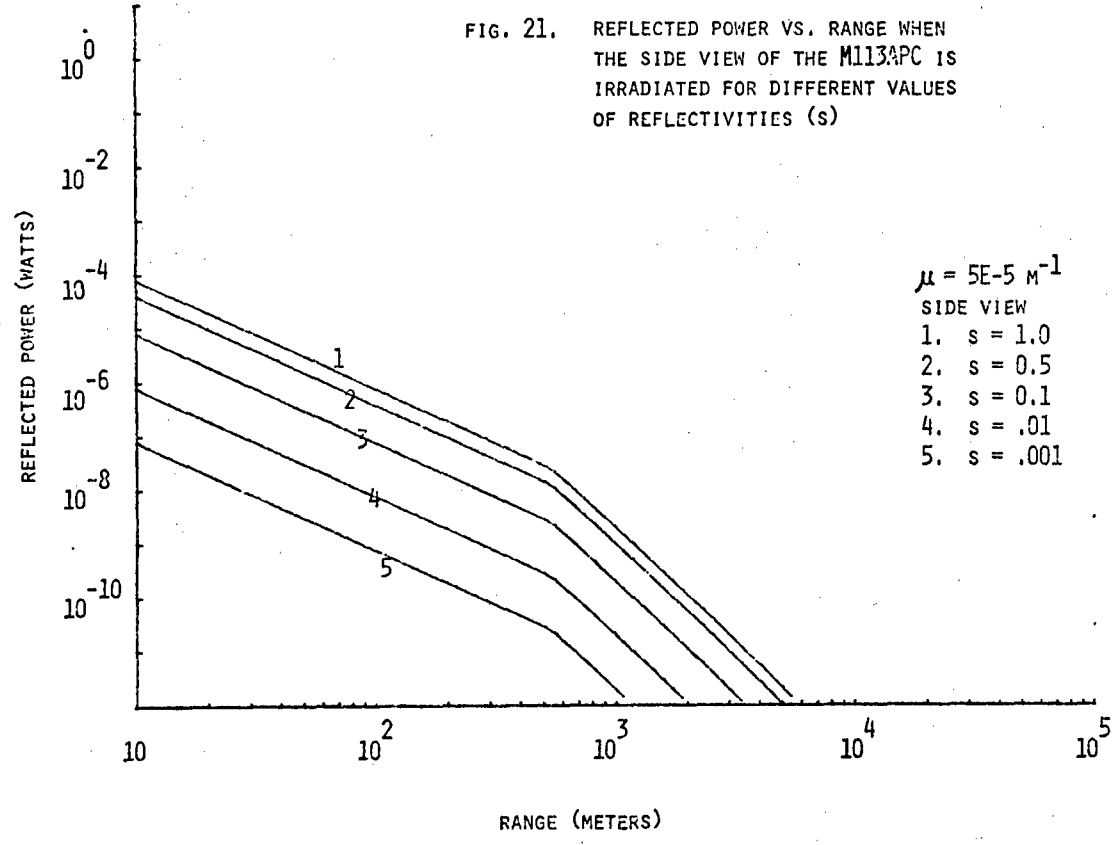

FIG. 21. REFLECTED POWER VS. RANGE WHEN THE SIDE VIEW OF THE M113APC IS IRRADIATED FOR DIFFERENT VALUES OF REFLECTIVITIES (s)

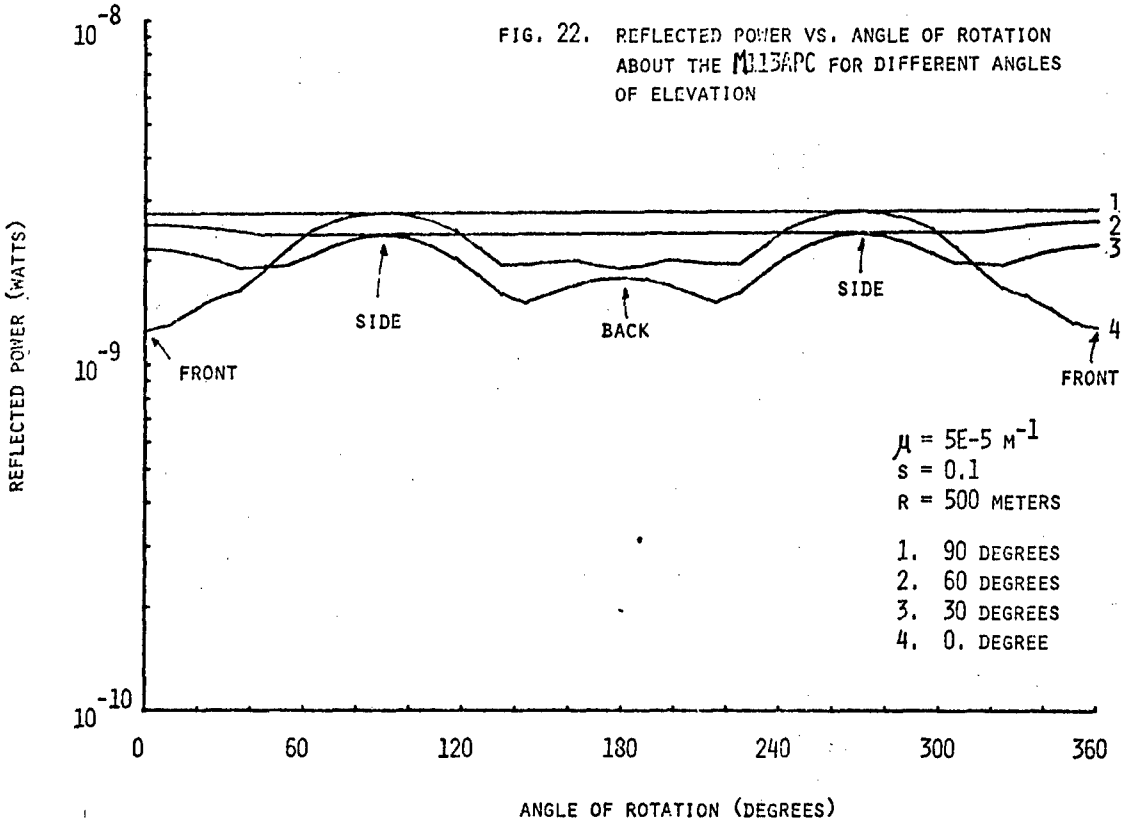

FIG. 22. REFLECTED POWER VS. ANGLE OF ROTATION ABOUT THE M113APC FOR DIFFERENT ANGLES OF ELEVATION

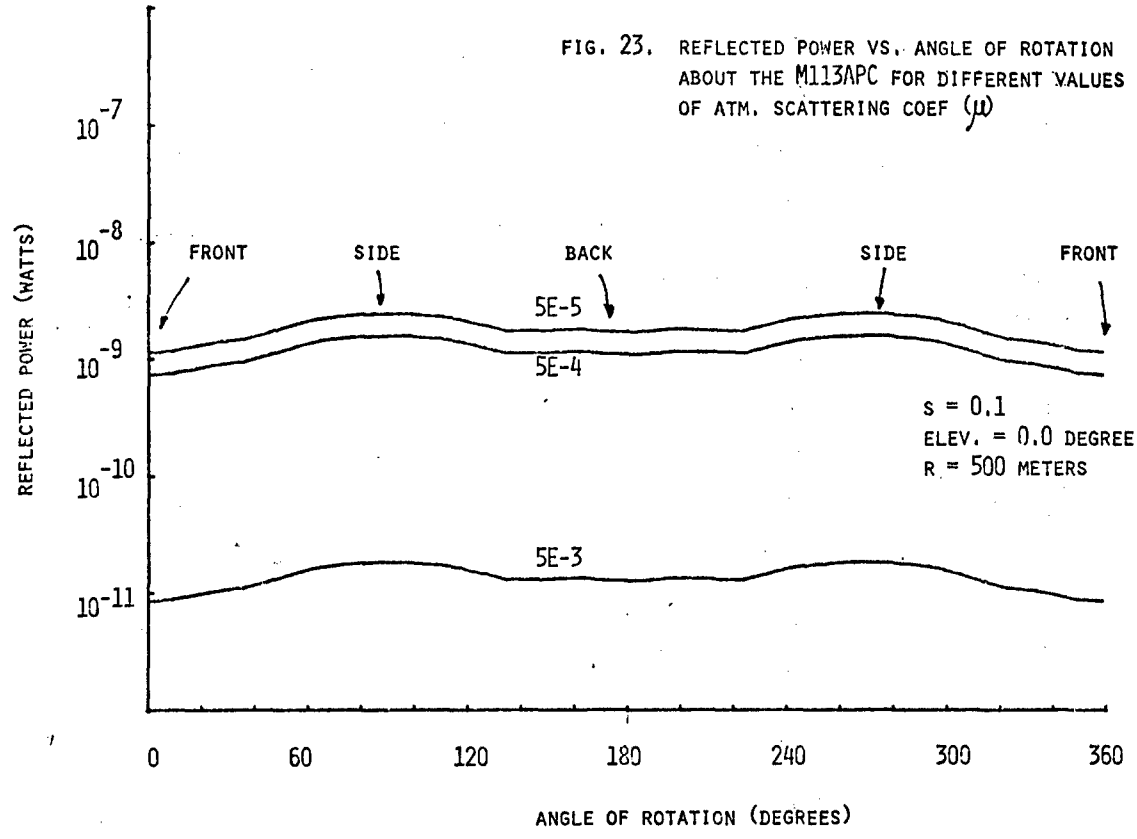

FIG. 23. REFLECTED POWER VS. ANGLE OF ROTATION ABOUT THE M113APC FOR DIFFERENT VALUES OF ATM. SCATTERING COEF (μ)

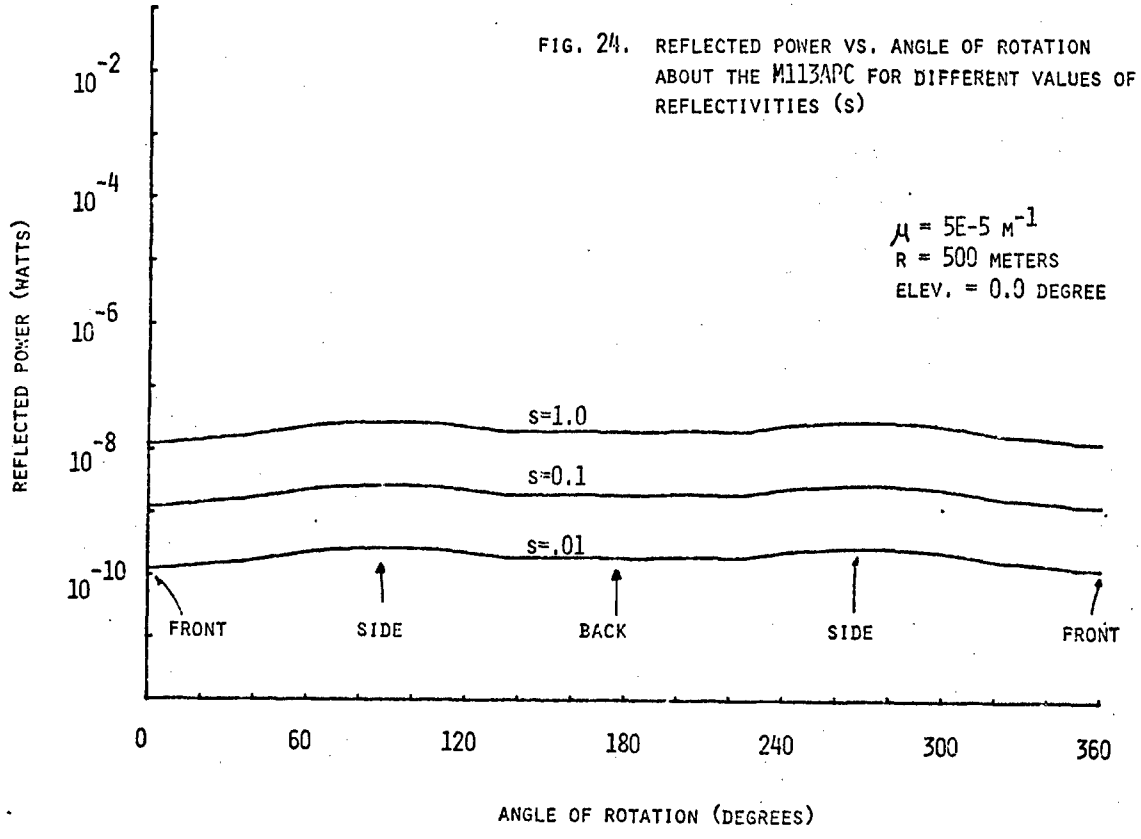

FIG. 24. REFLECTED POWER VS. ANGLE OF ROTATION ABOUT THE M113APC FOR DIFFERENT VALUES OF REFLECTIVITIES (s)

FIG. 25. REFLECTED POWER VS. ANGLE OF ROTATION ABOUT THE M113APC FOR DIFFERENT VALUES OF R

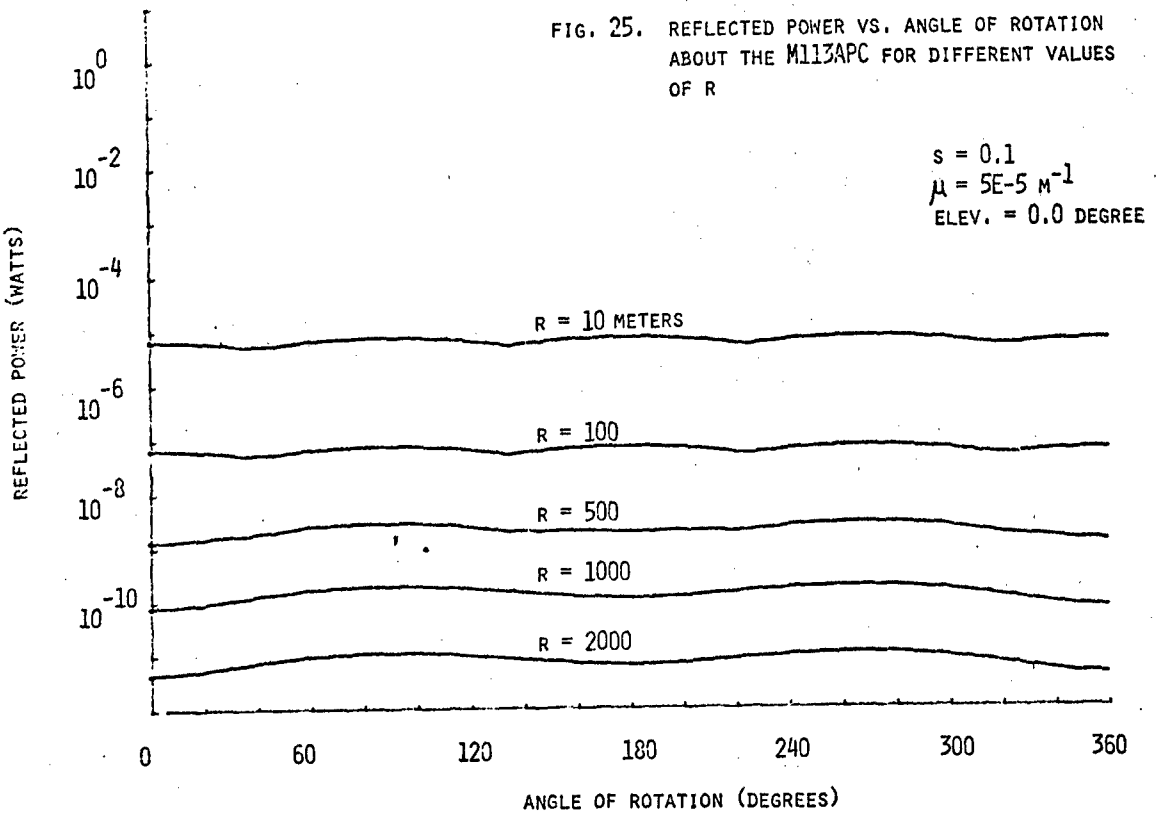

FIG. 26. REFLECTED POWER VS. RANGE FOR DIFFERENT VIEWS OF THE M113APC

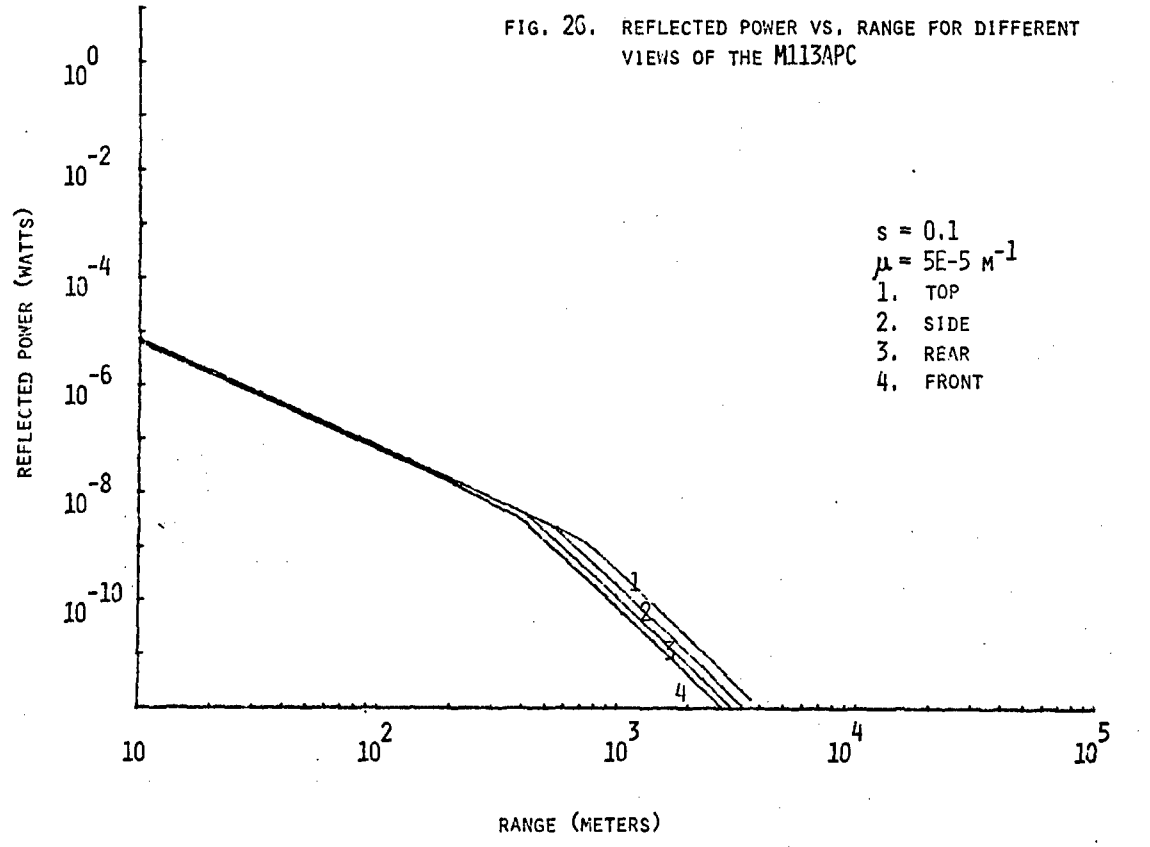

FIG. 27. REFLECTED POWER VS. RANGE WHEN THE M35A TRUCK IS IRRADIATED FOR DIFFERENT VALUES OF μ

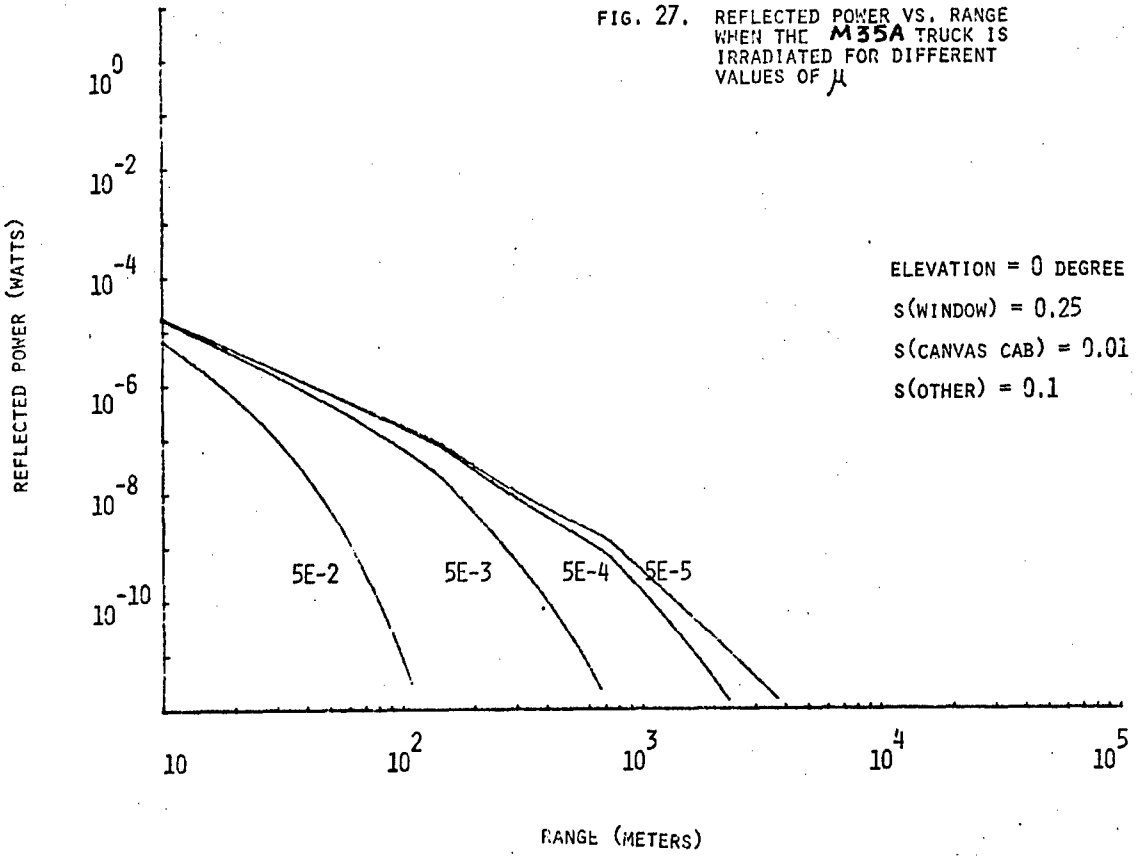

FIG. 28. REFLECTED POWER VS. RANGE WHEN THE M35A TRUCK IS IRRADIATED FOR DIFFERENT VALUES OF S

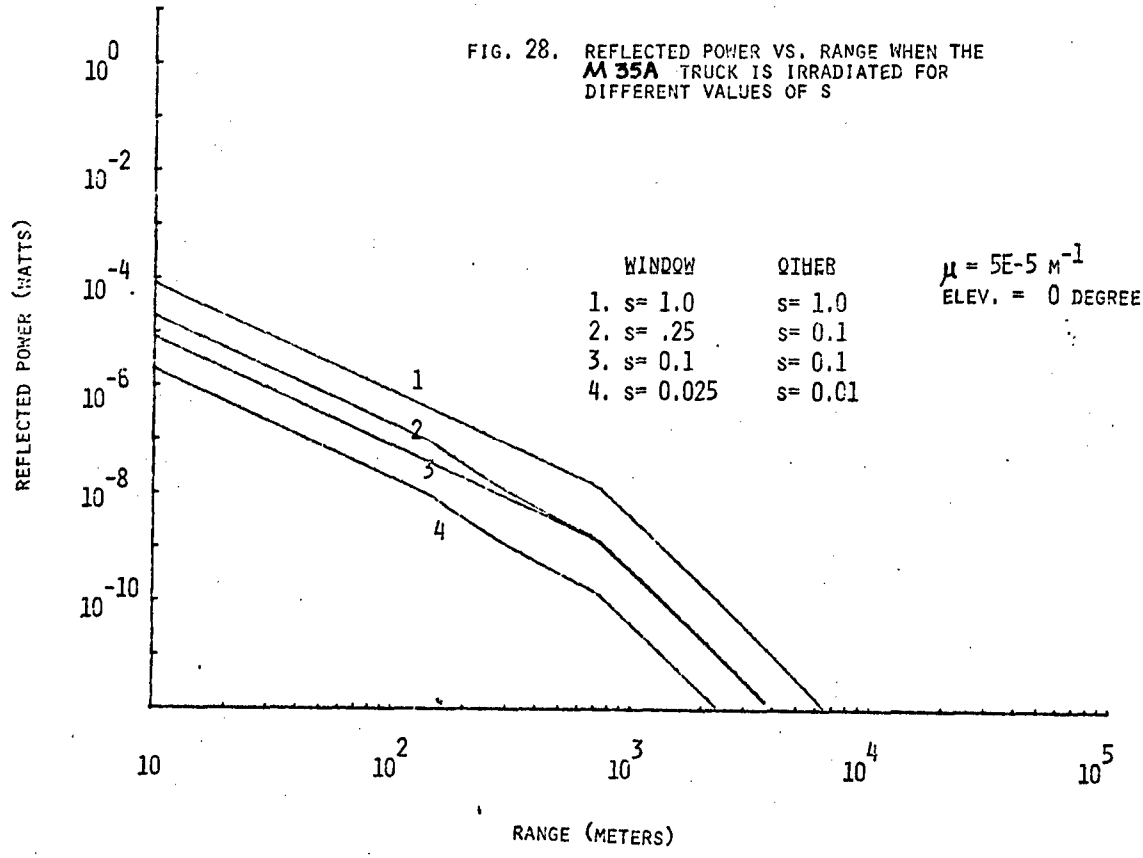

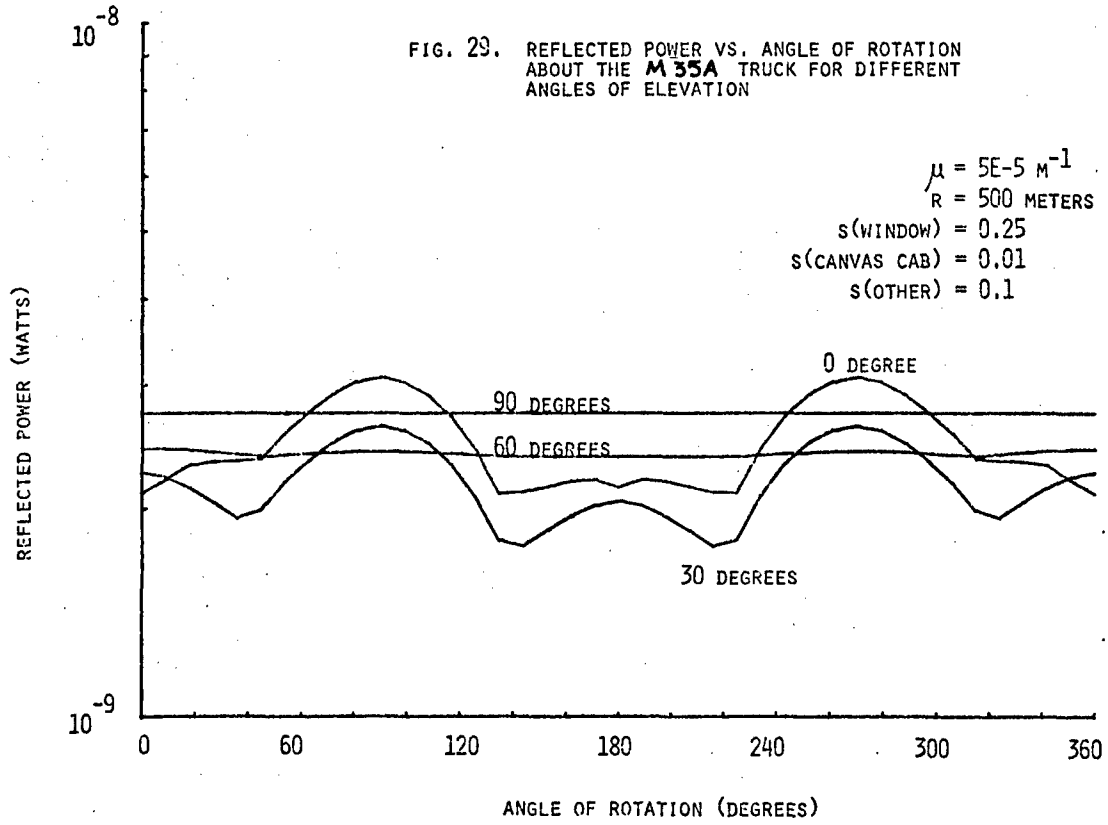

FIG. 29. REFLECTED POWER VS. ANGLE OF ROTATION ABOUT THE M35A TRUCK FOR DIFFERENT ANGLES OF ELEVATION

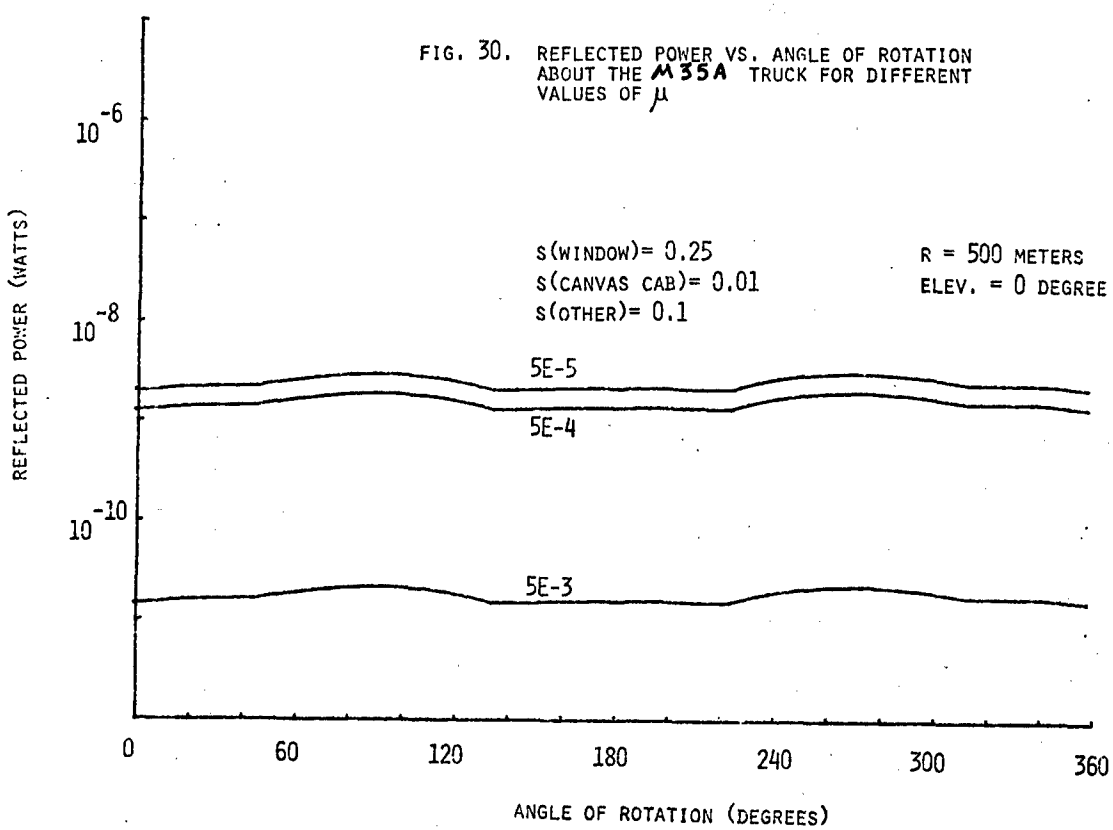

FIG. 30. REFLECTED POWER VS. ANGLE OF ROTATION ABOUT THE M35A TRUCK FOR DIFFERENT VALUES OF μ

FIG. 31. REFLECTED POWER VS. ANGLE OF ROTATION ABOUT THE M35A TRUCK FOR DIFFERENT VALUES OF S

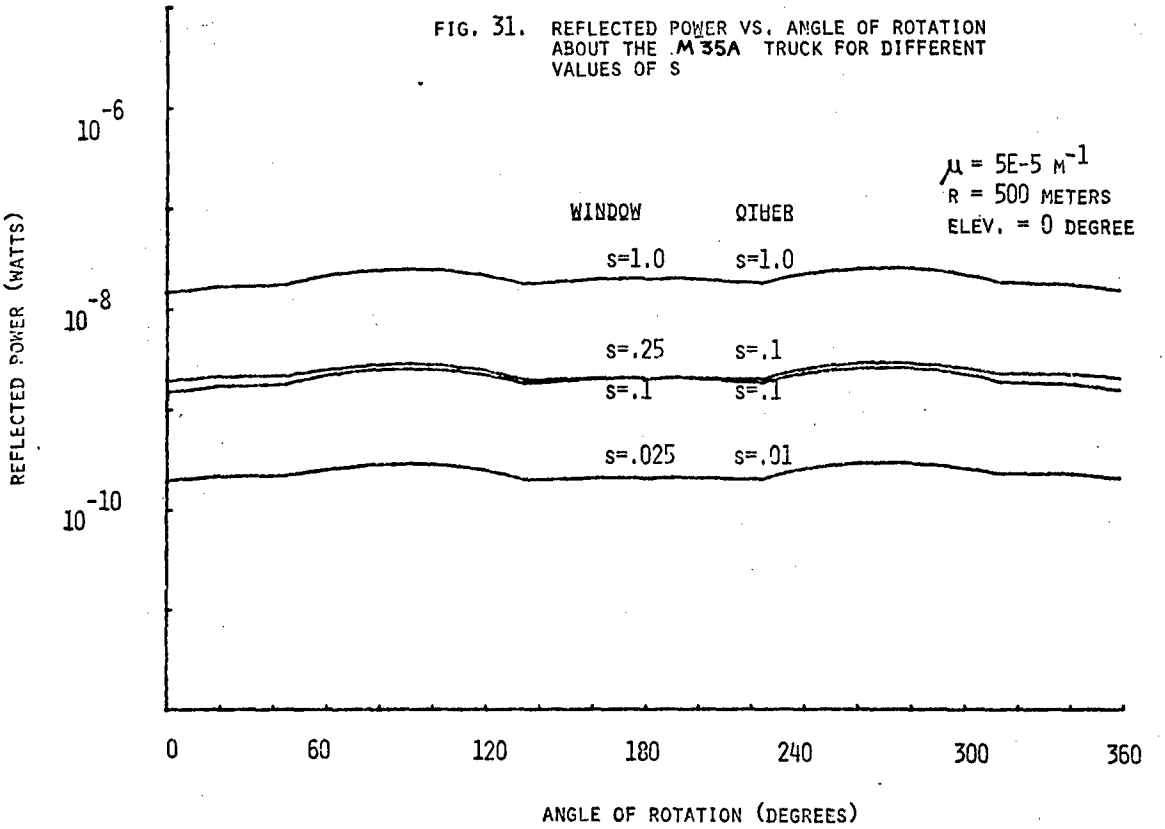

FIG. 32. REFLECTED POWER VS. ANGLE OF ROTATION ABOUT THE M35A TRUCK FOR DIFFERENT VALUES OF R

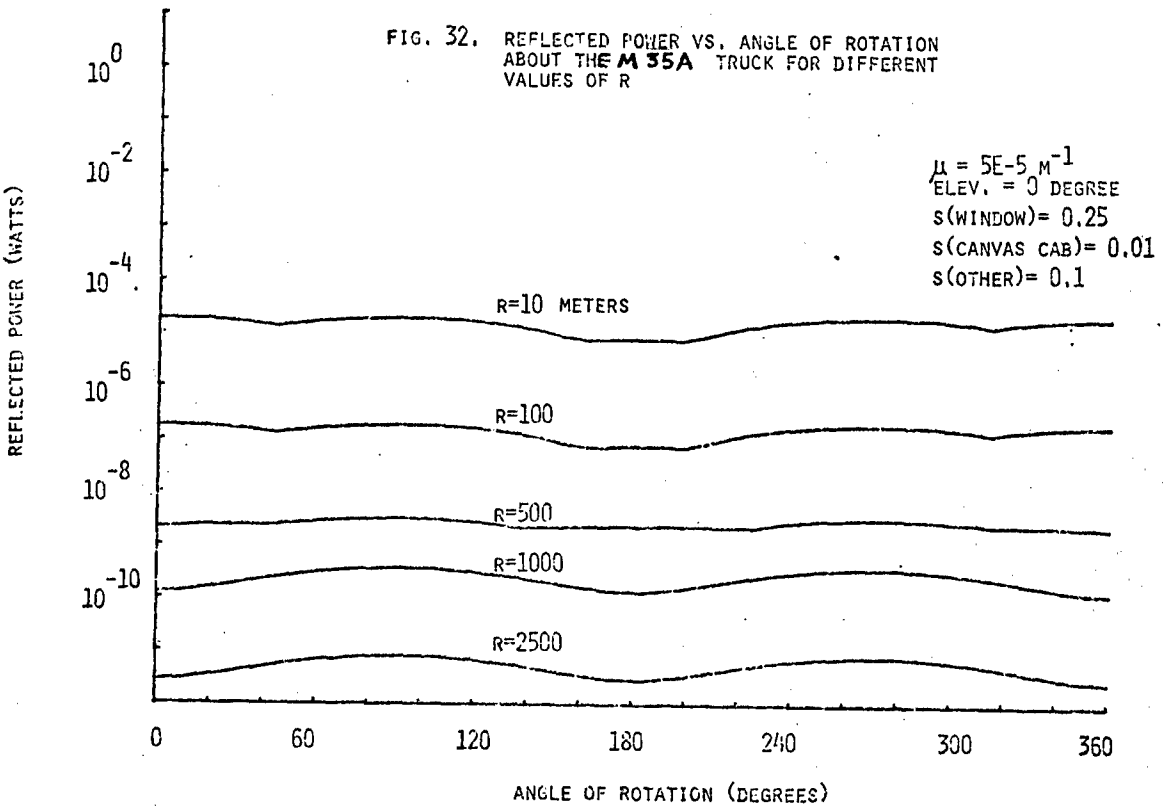

FIG. 33. REFLECTED POWER VS. RANGE FOR DIFFERENT VIEWS OF THE M35A TRUCK

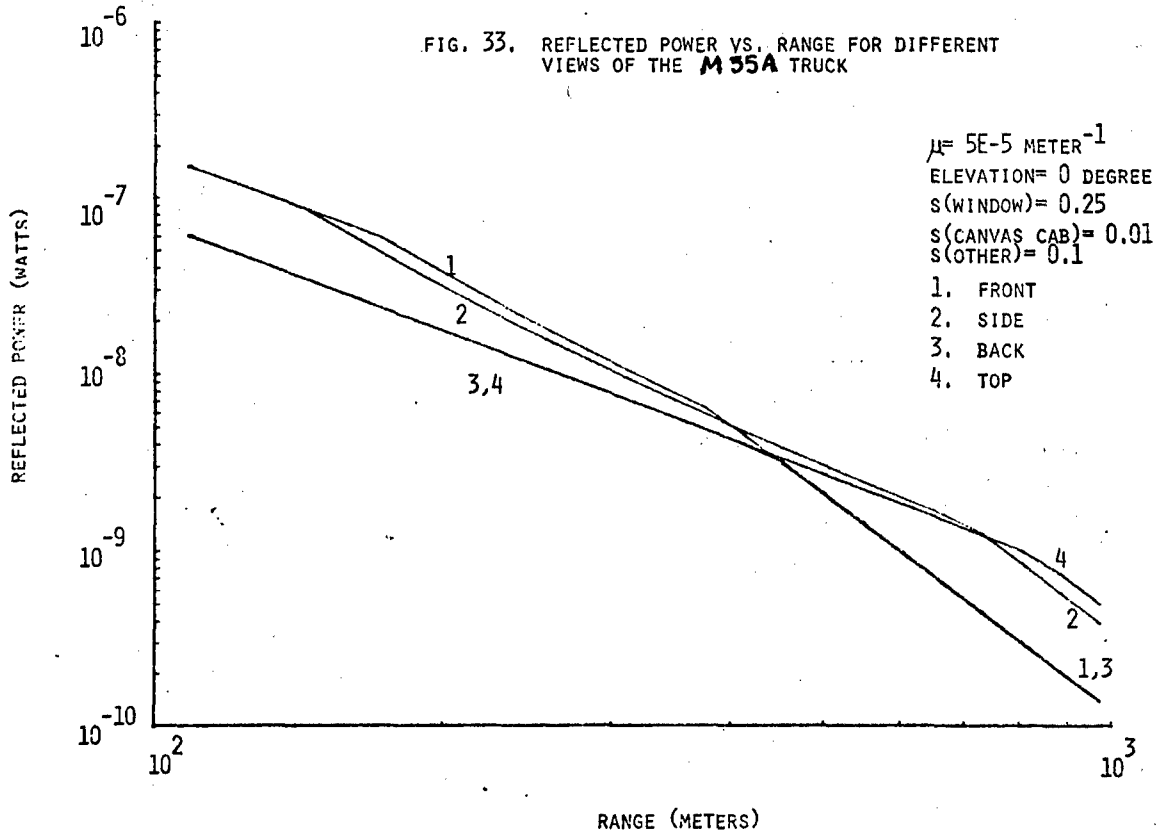

FIG. 34. REFLECTED POWER VS. RANGE WHEN THE FRONT VIEW OF THE M60A1 IS IRRADIATED FOR DIFFERENT VALUES OF μ

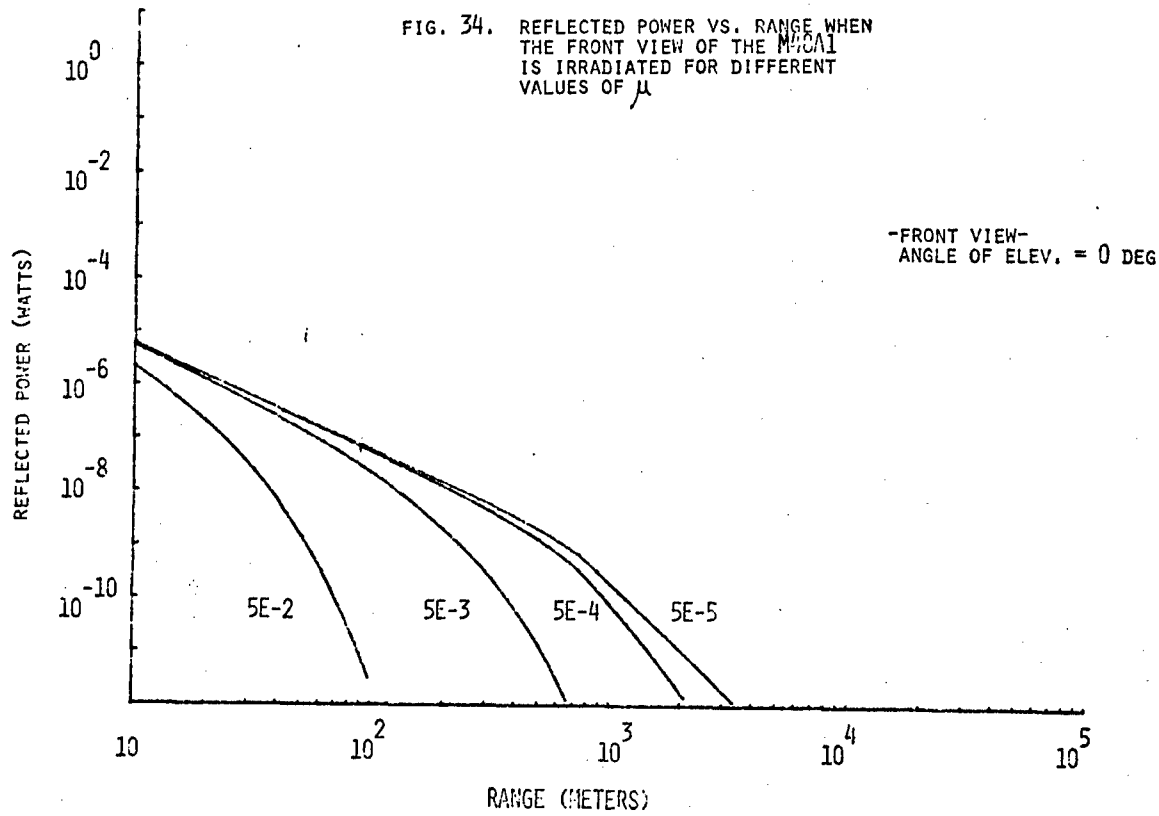

FIG. 35. REFLECTED POWER VS. RANGE WHEN THE FRONT VIEW OF THE M48A1 IS IRRADIATED FOR DIFFERENT VALUES OF S

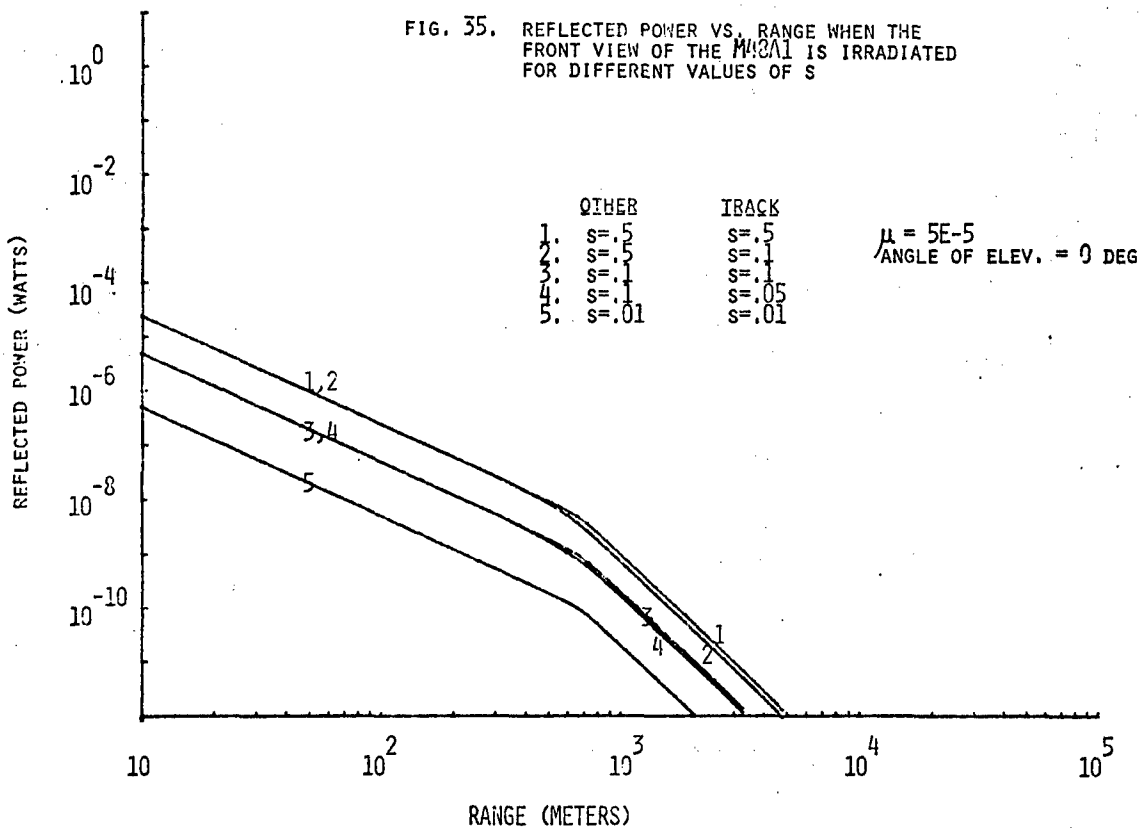

FIG. 36. REFLECTED POWER VS. RANGE FOR DIFFERENT VIEWS OF THE M48A1

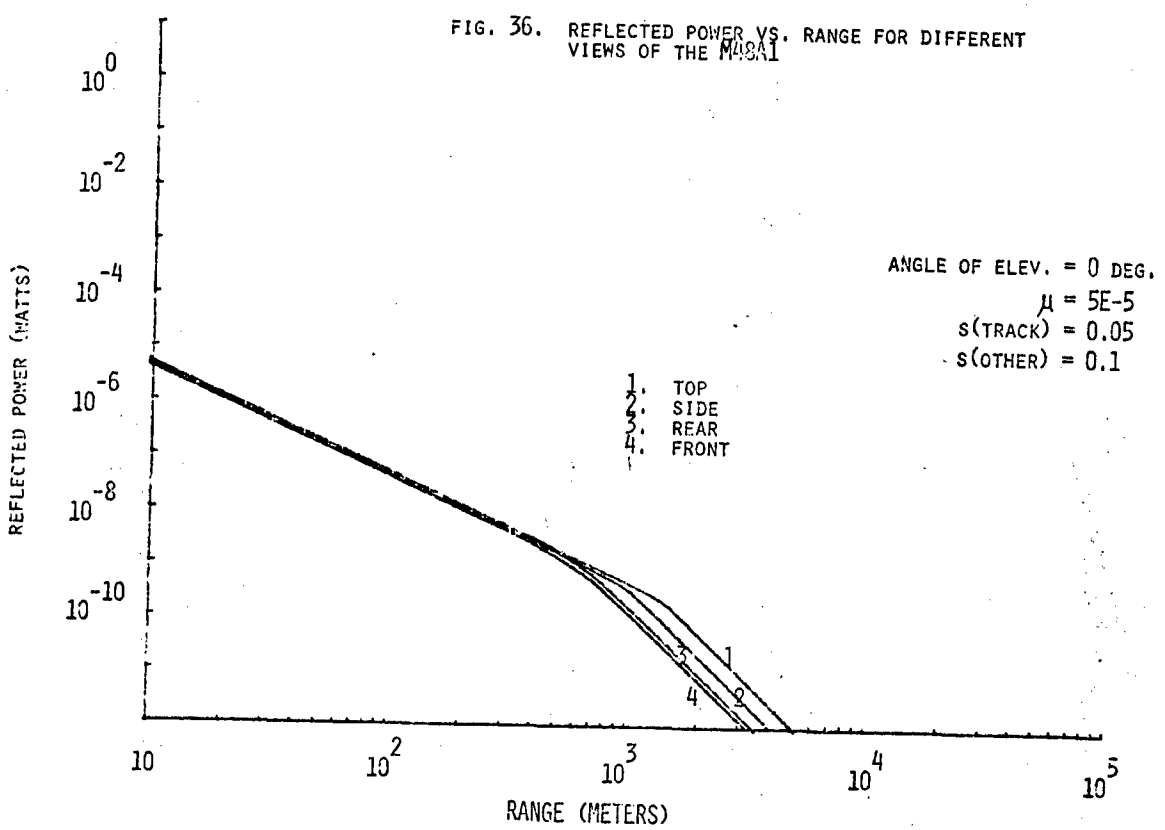

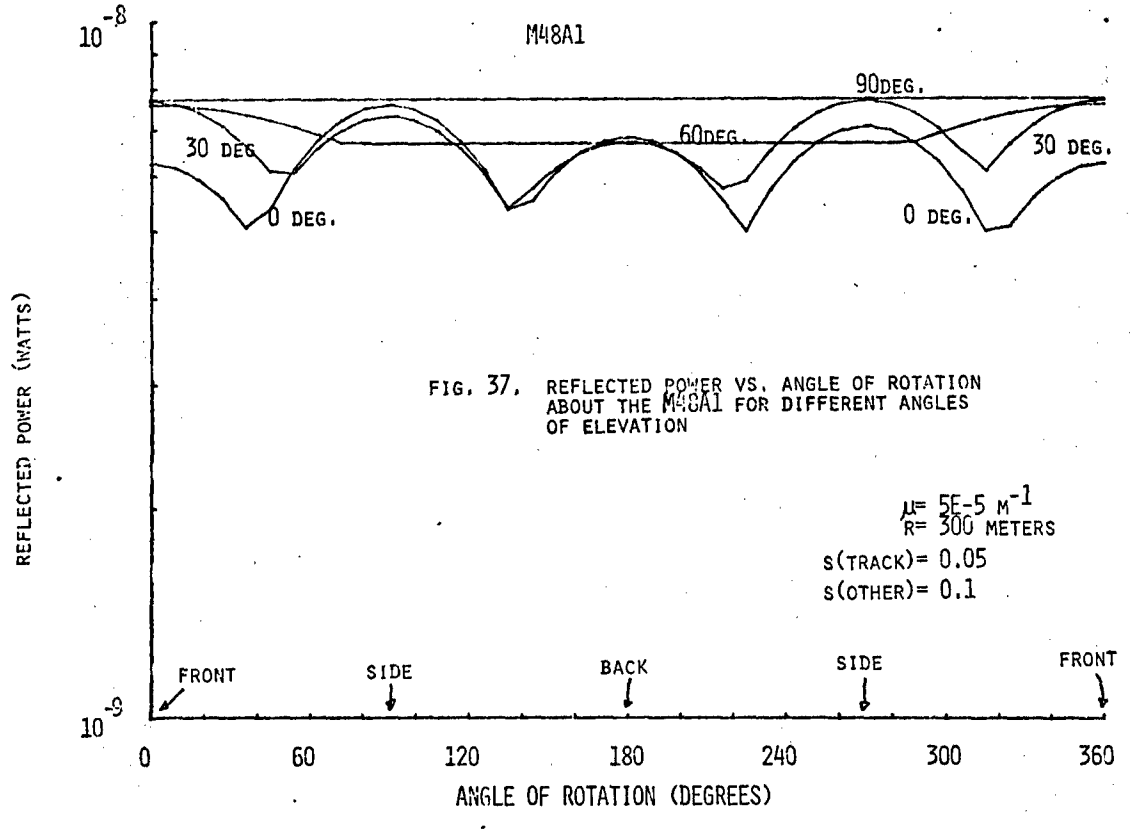

FIG. 37. REFLECTED POWER VS. ANGLE OF ROTATION ABOUT THE M48A1 FOR DIFFERENT ANGLES OF ELEVATION

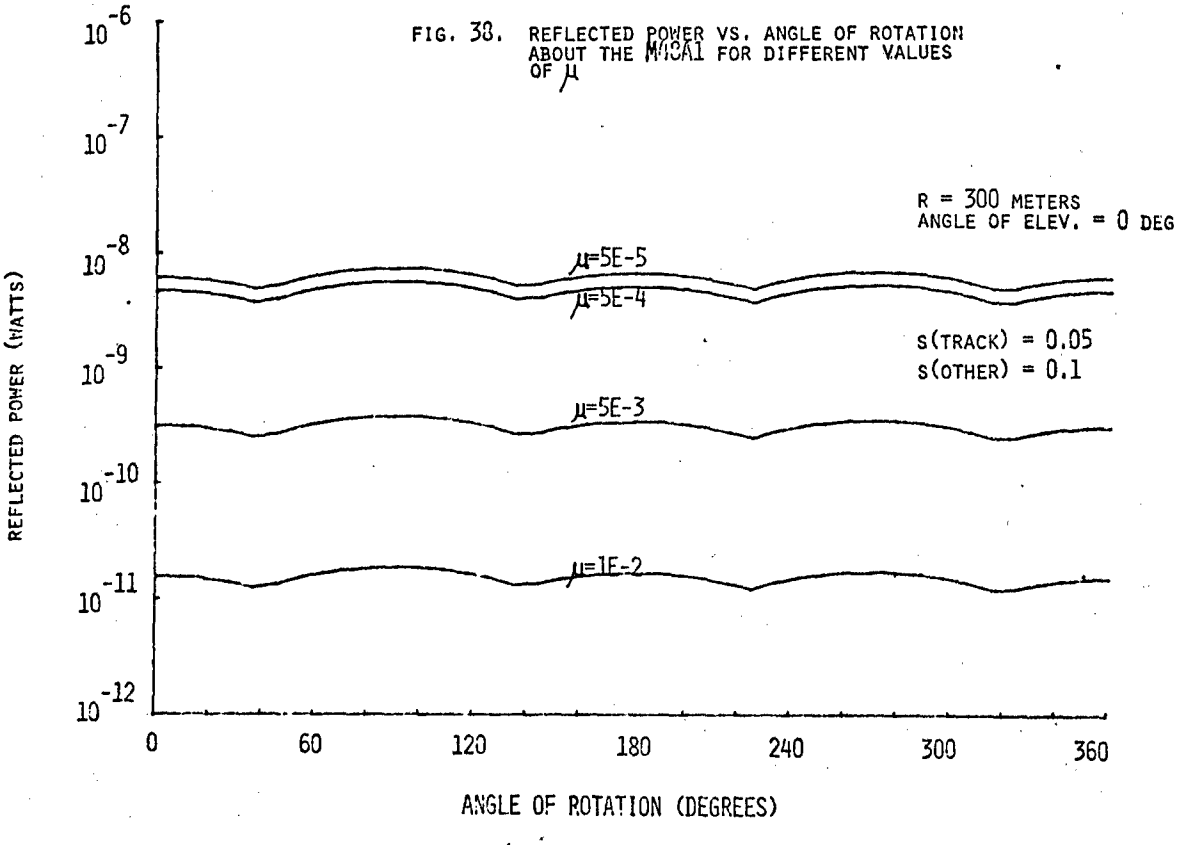

FIG. 38. REFLECTED POWER VS. ANGLE OF ROTATION ABOUT THE M48A1 FOR DIFFERENT VALUES OF μ

FIG. 39. REFLECTED POWER VS. ANGLE OF ROTATION ABOUT THE M48A1 FOR DIFFERENT VALUES OF S

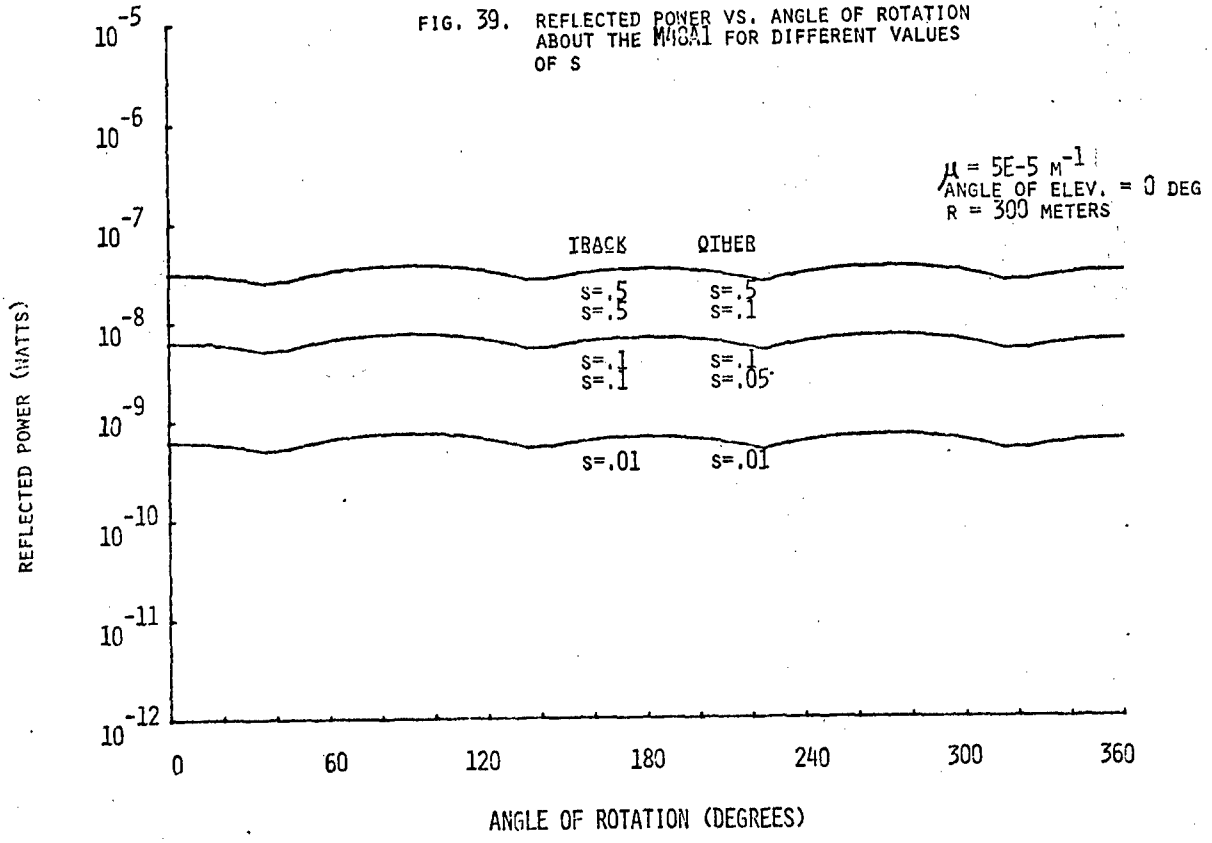

FIG. 40. REFLECTED POWER VS. ANGLE OF ROTATION ABOUT THE M48A1 FOR DIFFERENT VALUES OF R

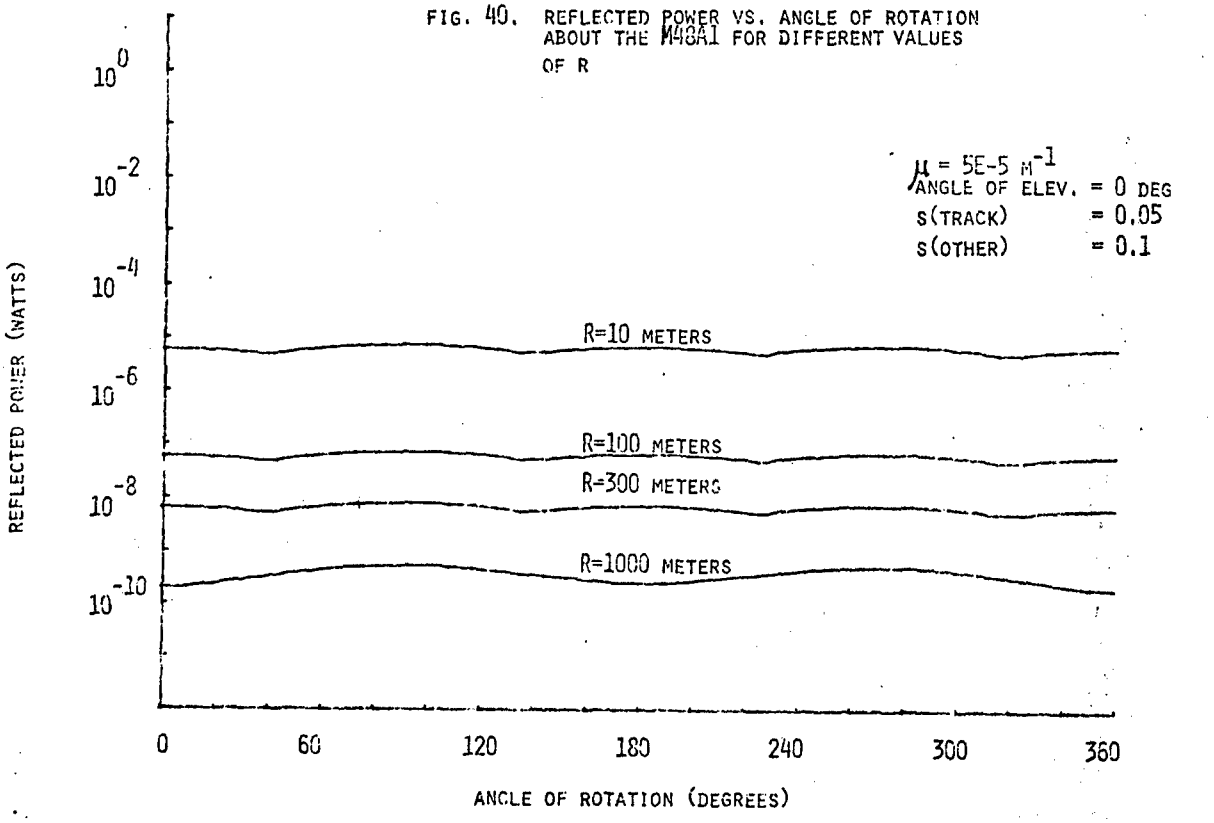

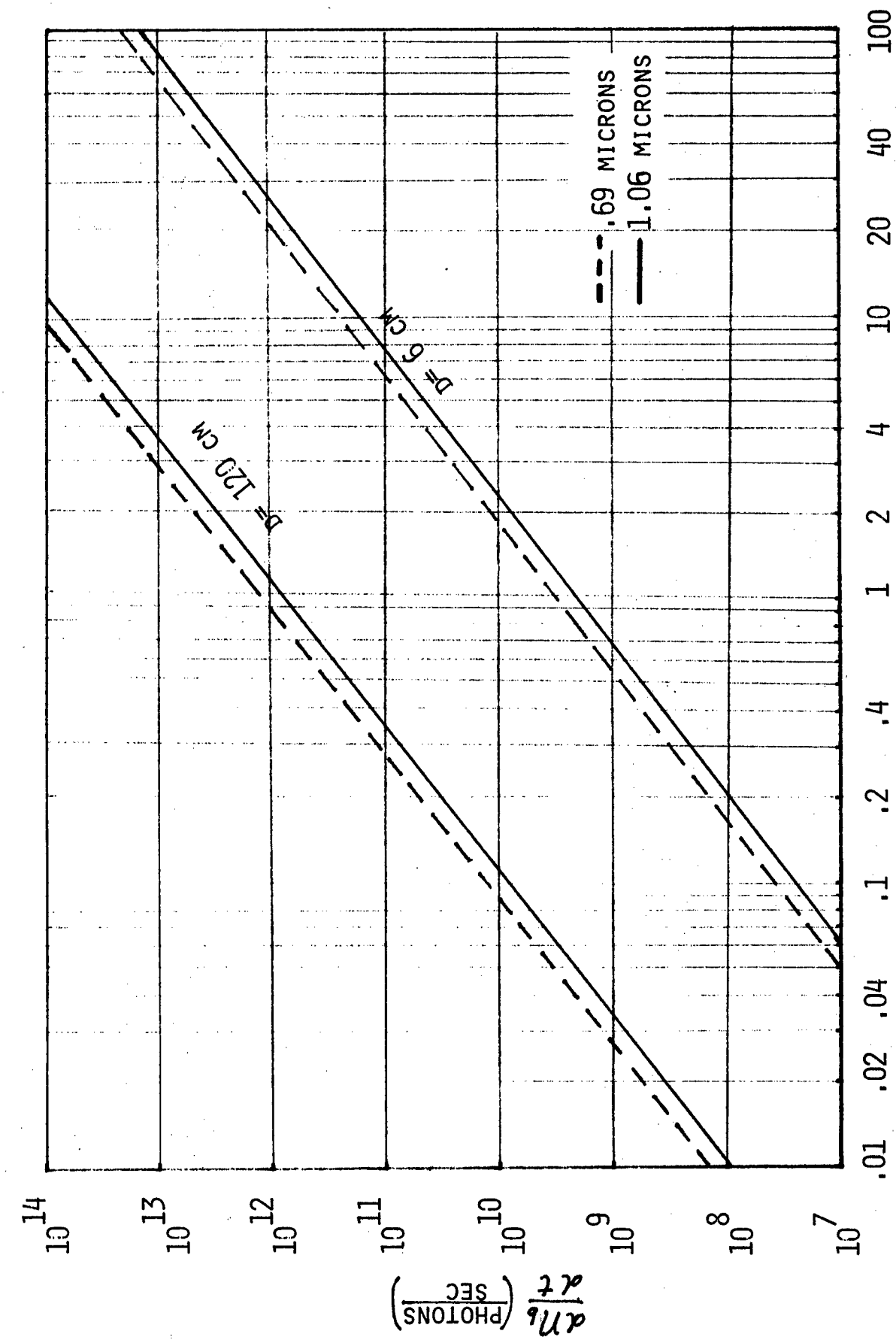

Fig. 41. Plot of solar background photon flux vs. field of view[28]

DISTRIBUTION LIST

	NO. OF COPIES
Commander US Army Tank-Automotive Research and Development Command	
ATTN: DRDTA-RHR	8
DRCPM-M113	1
DRCPM-M60-TP	1
Warren, MI 48090	
Commander US Army Mobility Equipment Research and Development Command	
ATTN: DRXFB-R	1
Fort Belvoir, VA 22060	
Commander Defense Documentation Center Cameron Station	8
Alexandria, VA 22314	
Commander US Army Training and Doctrine Command	
ATTN: ATCD-PM	1
Fort Monroe, VA 23651	
Commander US Army Combined Arms Combat Developments Activity	
ATTN: ATCA-CCC-S	1
Fort Leavenworth, KS 66027	

	NO. OF COPIES
Commander US Army Missile Research and Development Command ATTN: DRSMI-RR Redstone Arsenal, AL 35809	1
Commander Rock Island Arsenal ATTN: SARRI-LPL Rock Island, IL 61201	1
Commander TRADOC Combined Arms Test Activity ATTN: ATCAR-CSS-SE Fort Hood, TX 76544	1
Commander US Army Combat Development Experimentation Center ATTN: ATEC-PPA-M Fort Ord, CA 93940	1
Project Manager, Smoke ATTN: DRCPM-SMK Aberdeen Proving Ground, MD 21005	1
President US Army Armor and Engineer Board ATTN: ATZK-AE-AR Fort Knox, KY 40121	1
Director US Army TRADOC Analysis Activity ATTN: ATEC-PPA-M White Sands, NM 88002	1